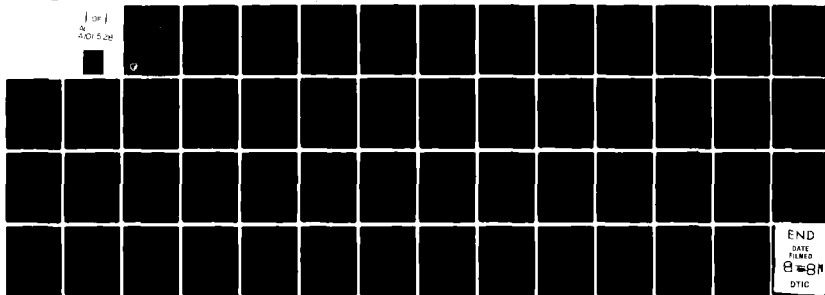


AD-A101 528 ARMY ELECTRONICS RESEARCH AND DEVELOPMENT COMMAND WS--ETC F/8 4/1
SENSITIVITY ANALYSIS OF A MESOSCALE MOISTURE MODEL.(U)
MAR 81 J L COGAN
UNCLASSIFIED ERADCOM/ASL-TR-0079 NL

1 of 1
AD-A101 528



ASL-TR-0079✓

LEVEL II

6

AD

Reports Control Symbol
OSD 1366

AD A101528

SENSITIVITY ANALYSIS OF A MESOSCALE MOISTURE MODEL

MARCH 1981

DTIC
JUL 17 1981

By
JAMES L. COGAN

Approved for public release; distribution unlimited



US Army Electronics Research and Development Command
ATMOSPHERIC SCIENCES LABORATORY
White Sands Missile Range, NM 88002

81 4 17 1981

NOTICES

Disclaimers

The findings in this report are not to be construed as an official Department of the Army position, unless so designated by other authorized documents.

The citation of trade names and names of manufacturers in this report is not to be construed as official Government indorsement or approval of commercial products or services referenced herein.

Disposition

Destroy this report when it is no longer needed. Do not return it to the originator.

ERRATA SHEET FOR

ASL-TR-0079

Sensitivity Analysis of a Mesoscale

Moisture Model

Page 5 Figure 4a, last line of caption. Change "2b" to "3a."

Page 9 Equation in para a is changed as follows:

$$\pi = c_p \left(\frac{p}{p_0} \right)^{R/c_p} \quad \theta_v = T_v \left(\frac{p_0}{p} \right)^{R/c_p}$$

Para b, fifth line. Footnote reference to Cogan⁹ is shown on page 11.

Page 25 Figure 4a, fourth line of caption. Change "2b" to "3a."

SECURITY CLASSIFICATION OF THIS PAGE (When Data Entered)

REPORT DOCUMENTATION PAGE

READ INSTRUCTIONS
BEFORE COMPLETING FORM

1. REPORT NUMBER

ASL-TR-0079

2. GOVT ACCESSION NO.

AD-A101

3. RECIPIENT'S CATALOG NUMBER

528

4. TITLE (and Subtitle)

SENSITIVITY ANALYSIS OF A MESOSCALE
MOISTURE MODEL

5. TYPE OF REPORT & PERIOD COVERED

Final Report

6. PERFORMING ORG. REPORT NUMBER

7. AUTHOR(s)

James L. Cogan

8. CONTRACT OR GRANT NUMBER(s)

9. PERFORMING ORGANIZATION NAME AND ADDRESS

US Army Atmospheric Sciences Laboratory
White Sands Missile Range, NM 88002

10. PROGRAM ELEMENT, PROJECT, TASK
AREA & WORK UNIT NUMBERS

DA Task No. 11161102B53A

11. CONTROLLING OFFICE NAME AND ADDRESS

US Army Electronics Research
and Development Command
Adelphi, MD 20783

12. REPORT DATE

March 1981

13. NUMBER OF PAGES

53

14. MONITORING AGENCY NAME & ADDRESS (if different from Controlling Office)

15. SECURITY CLASS. (of this report)

Unclassified

16. DECLASSIFICATION/DOWNGRADING
SCHEDULE

16. DISTRIBUTION STATEMENT (of this Report)

Approved for public release; distribution unlimited.

17. DISTRIBUTION STATEMENT (of the abstract entered in Block 20, if different from Report)

18. SUPPLEMENTARY NOTES

19. KEY WORDS (Continue on reverse side if necessary and identify by block number)

Mesoscale models
Moisture models
Meteorology
Sensitivity analysis

Atmospheric water
Precipitation
Terrain effects

20. ABSTRACT (Continue on reverse side if necessary and identify by block number)

A two-dimensional mesoscale moisture model is described briefly and some recent modifications are outlined. Results from the model were computed for a variety of atmospheres and terrain types. A limited sensitivity analysis showed the effect of different model input parameters on meteorological variables for one vertical column through the atmosphere at a central horizontal grid point. A detailed analysis of selected cases for the entire domain of the model indicated the effect of input parameters on vertical velocity,

421603

20. ABSTRACT (cont)

precipitation amount, and precipitation rate. For one set of input parameters, analyses were performed of the variation of vertical velocity and precipitation every 2 hours for a 12-hour period. An example of a potential application to electro-optical algorithms is discussed and suggestions are made for future work.

CONTENTS

LIST OF TABLES.....	4
LIST OF FIGURES.....	5
1. INTRODUCTION.....	7
2. MODEL DESCRIPTION.....	8
3. MODEL MODIFICATIONS.....	11
4. RESULTS AND SAMPLE OUTPUT.....	11
5. CROSS-SECTIONAL ANALYSES.....	13
5.1 Variation of Input Parameters at Constant Model Time.....	14
5.2 Time Variation of Results.....	16
6. SUGGESTIONS AND CONCLUSION.....	17
TABLE	20
FIGURES	22
REFERENCES.....	35
APPENDIX	36
PROGNOSTIC EQUATIONS.....	36
DIAGNOSTIC EQUATIONS.....	38

Accession For	
NTIS GRA&I	<input checked="checked" type="checkbox"/>
DTIC TAB	<input type="checkbox"/>
Unannounced	<input type="checkbox"/>
Justification	
By	
DTIC	
A	

LIST OF TABLES

1. Values of Seven Variables Computed by the 2DMM for Twenty Sets
of Model Input Parameters..... 20

LIST OF FIGURES

1. Sounding values for input into the 2DMM. Z is height, T is temperature, RH is relative humidity, and U is the east-west component of wind where positive flow is from west to east..... 22

- 2a. Cross section of vertical velocity (w) with coordinates of height and horizontal distance (x) for the case of flat terrain and a moist atmosphere (see figure 1) at 720 minutes. Data are plotted for every odd grid point at 16 vertical levels. W is in cm s^{-1} 23

- 2b. Graph of accumulated precipitation (AP) plotted against horizontal distance (x) for the moist atmosphere and flat terrain. Total AP is the sum of all grid point values..... 23

- 3a. Cross section of vertical velocity (w) with coordinates of height and horizontal distance (x). The same as 2a except that the temperature (T) sounding was modified so that $T = T + 5^\circ\text{C}$ at 0-1 km, $T = T + 3^\circ\text{C}$ at 2 km, and $T = T + 1.5^\circ\text{C}$ at 3 km..... 24

- 3b. Same as figure 2.b but with the initial vertical profile of temperature (T) modified so that $T = T + 5^\circ\text{C}$ at 0-1 km, $T = T + 3^\circ\text{C}$ at 2 km, and $T = T + 1.5^\circ\text{C}$ at 3 km..... 24

- 4a. Cross section of vertical velocity (w) with coordinates of height and distance (x). The same as 2a except that sinusoidal mountain terrain was used (indicated on the cross section) and the initial temperature sounding was modified as for 2b (and indicated on the cross section)..... 25

- 4b. Same as figure 2b but with the sinusoidal mountain and the initial vertical profile of temperature (T) modified as in 3b. The location of the sinusoidal mountain is indicated by the double ended arrow..... 25

- 5a. Cross section of vertical velocity (w) with coordinates of height and horizontal distance (x). The same as 2a except that wedge terrain was used (maximum height of terrain is 0.96 km at grid point 25)..... 26

- 5b. Same as figure 2b but with wedge terrain (maximum height of terrain is 0.96 km at grid point 25)..... 26

- 6a. Cross section of vertical velocity (w) with coordinates of height and horizontal distance (x). The same as 2a except that the unmodified version of the 2DMM was used with the sinusoidal mountain terrain..... 27

- 6b. Same as 2b except that the unmodified version was used with the sinusoidal mountain. The location of the mountain is indicated by the double ended arrow..... 27

7. Graphs of accumulated precipitation (AP) plotted against horizontal distance (x). Model input parameters are listed on the separate graphs. Total AP is the sum of all grid point values..... 28

8. Cross section of vertical velocity (w) with coordinates of height and horizontal distance (x), and graphs of accumulated precipitation (AP) and precipitation rate (PR), using the input parameters of the sinusoidal mountain and a moist atmosphere (see figure 1) at 120 minutes. The cross hatched area on the cross section (a) and the double ended arrow on the graphs (b, c) indicate the location of the mountain. W is in cm s^{-1} . Total AP is the sum of all the grid point values. Horizontal distance is in km and grid point..... 29

9. (a) Cross section of vertical velocity (w) with coordinates of height and horizontal distance (x), and (b, c) graphs of accumulated precipitation (AP) and precipitation rate (PR). The same as figure 8 but for 240 minutes..... 30

10. (a) Cross section of vertical velocity (w) with coordinates of height and distance horizontal (x), and (b, c) graphs of accumulated precipitation (AP) and precipitation rate (PR). The same as figure 8 but for 360 minutes..... 31

11. (a) Cross section of vertical velocity (w) with coordinates of height and horizontal distance (x), and (b, c) graphs of accumulated precipitation (AP) and precipitation rate (PR). The same as figure 8 but for 480 minutes..... 32

12. (a) Cross section of vertical velocity (w) with coordinates of height and horizontal distance (x), and (b, c) graphs of accumulated precipitation (AP) and precipitation rate (PR). The same as figure 8 but for 600 minutes..... 33

13. (a) Cross section of vertical velocity (w) with coordinates of height and horizontal distance (x), and (b, c) graphs of accumulated precipitation (AP) and precipitation rate (PR). The same as figure 8 but for 720 minutes..... 34

1. INTRODUCTION

The description of the distribution and the characteristics of water in the atmosphere generally has been approached from two opposing points of view. Operational models produce gross measures over relatively large areas, while specialized models address manifestations such as fog, clouds, or precipitation of a specific type or at a specific location. However, there has been no unified set of models which handles atmospheric water in a manner that has broad applicability over a relatively small area.

The requirements for a structure of a unified system of models are discussed in some detail by Kreitzberg et al.¹ Cionco² shows how such a system could provide necessary atmospheric information for Army applications. This latter report also describes the general characteristics of a nested set of models and briefly outlines the tasks and requirements for their development and implementation. A sensitivity analysis of a two-dimensional moisture model (2DMM) can lead to an understanding of moisture models and their usefulness and has the potential to produce preliminary information that will be of use as input to algorithms for modeling atmospheric effects on electro-optical (EO) systems. Such an analysis can provide the necessary understanding and experience to begin to work with a far more complex set of nested models in three dimensions (three-dimensional moisture model, [3DMM]) of the type described by Cionco² and Kreitzberg et al.¹ This latter reference includes an extensive bibliography on atmospheric moisture models, their applications, and closely related topics. The application of output from a 3DMM to EO algorithms is noted by Cionco² and mentioned briefly in this report.

¹C. W. Kreitzberg, W. D. Mount, and B. R. Fow, 1979, Preliminary Evaluation of Meteorological Models for Moisture Depiction and Prediction for Electro-Optical Applications, Contract DAAG29-76-D-0100, US Army Research Office, PO Box 12211, Research Triangle Park, NC

²R. M. Cionco, 1980, Moisture Analysis, Depiction and Prediction System of Models: Description of the ASL Program, Internal Report, US Army Atmospheric Sciences Laboratory, White Sands Missile Range, NM

The 2DMM was originally developed by Kreitzberg et al³ and modified and discussed by Perkey,⁴ Kreitzberg and Perkey,^{5 6} and Loveland.* Results of a sensitivity analysis of the 2DMM are presented herein and briefly discussed. This report also briefly outlines some basic facets of the model and presents a short discussion on the possible use of results from the 2DMM for a few of the algorithms in the Electro-Optical Systems Atmospheric Effects Library described by Duncan et al.⁷

2. MODEL DESCRIPTION

No attempt is made in this brief report to describe the 2DMM in detail, but this section provides a framework which may be filled in by referring to the

³C. W. Kreitzberg, D. J. Perkey, and J. E. Pinkerton, 1974, Mesoscale Modeling, Forecasting, and Remote Sensing Research, Project THEMIS Final Report, AFCRL-TR-74-0253, Department of Physics and Atmospheric Sciences, Drexel University, Philadelphia, PA. AD 784875

⁴D. J. Perkey, 1976, "A Description of Preliminary Results from a Fine-Mesh Model for Forecasting Quantitative Precipitation," Monthly Weather Rev., 104:1513-1525

⁵C. W. Kreitzberg and D. J. Perkey, 1976, "Release of Potential Instability: Part I. A sequential plume model within a hydrostatic primitive equation model," J Atmospheric Sci., 33:456-475

⁶C. W. Kreitzberg and D. J. Perkey, 1977, "Release of Potential Instability: Part II. The mechanism of convective/mesoscale interaction," J Atmospheric Sci., 34:1571-1595

*K. T. Loveland, 1980, Unpublished manuscripts on the two-dimensional, hydrostatic, primitive equation model, Department of Physics and Atmospheric Sciences, Drexel University, Philadelphia, PA, 238 pp

⁷L. D. Duncan et al, 1979, The Electro-Optical Systems Atmospheric Effects Library, Volume I, Technical Documentation. ASL-TR-0047, US Army Atmospheric Sciences Laboratory, White Sands Missile Range, NM

many papers on mesoscale modeling and related areas. Kreitzberg et al,³ Kreitzberg and Perkey,⁵ ⁶ Perkey,⁴ and Loveland* relate directly to the 2DMM, and the first four papers ³⁻⁶ contain many more references on this subject.

The 2DMM is a primitive equation model which assumes a hydrostatic atmosphere and has several nonstandard plus some more "ordinary" features as follows.*

a. Pressure (p) and virtual temperature (T_v) are replaced by the Exner function (π) and the virtual potential temperature (θ_v)

$$\pi = C_p \frac{p}{p_0} \left(\frac{R}{C_p} \right) \quad \theta_v = T_v \frac{p_0}{p} \left(\frac{R}{C_p} \right)$$

where C_p = specific heat at constant pressure and R is the gas constant for dry air.

b. The vertical coordinates are: (1) terrain following (σ_z) up to a height H, about halfway through the atmosphere in terms of mass (~3 to 5 km), and (2) height above sea level (z) at altitudes greater than H. Typical vertical resolution is about 1 km, but may vary with height to permit a higher resolution near the surface. Figure 1 of Cogan⁹ shows a sketch of the vertical coordinate system. Horizontal grid points are spaced evenly, typically 40 km, although the interval (ΔX) may be changed. There are 16 grid points in the vertical and 25 in the horizontal.

³C. W. Kreitzberg, D. J. Perkey, and J. E. Pinkerton, 1974, Mesoscale Modeling, Forecasting, and Remote Sensing Research, Project THEMIS Final Report, AFCRL-TR-74-0253, Department of Physics and Atmospheric Sciences, Drexel University, Philadelphia, PA. AD 784875

⁵C. W. Kreitzberg and D. J. Perkey, 1976, "Release of Potential Instability: Part I. A sequential plume model within a hydrostatic primitive equation model," J Atmospheric Sci, 33:456-475

⁶C. W. Kreitzberg and D. J. Perkey, 1977, "Release of Potential Instability: Part II. The mechanism of convective/mesoscale interaction," J Atmospheric Sci, 34:1571-1595

⁴D. J. Perkey, 1976, "A Description of Preliminary Results from a Fine-Mesh Model for Forecasting Quantitative Precipitation," Monthly Weather Rev, 104:1513-1525

*K. T. Loveland, 1980, Unpublished manuscripts on the two-dimensional, hydrostatic, primitive equation model, Department of Physics and Atmospheric Sciences, Drexel University, Philadelphia, PA, 238 pp

c. The model contains prognostic equations for the horizontal components of velocity (u, v) virtual potential temperature (θ_v), specific humidity (q), cloud water concentration (c), rain water concentration (r) and π at the top of the model (π_{top}). π below π_{top} is diagnosed hydrostatically by using an effective θ_v that accounts for the cloud water and precipitation loading. Vertical motion is calculated diagnostically from the continuity equation. A summary of diagnostic and prognostic equations is given in the appendix.

d. The finite difference scheme "is basically second-order centered in the vertical, fourth-order centered in the horizontal, and leapfrog in time with time filtering to avoid separation of solutions."

e. A "smoother-desmoother" smooths spatially to eliminate horizontal variations of u , v , θ_v , and π_{top} for wavelengths on the order of $2\Delta X$. Time averaging of the horizontal gradient of π allows for a longer time-step; for $\Delta X = 40$ km, the time-step is about 100 seconds.⁶

f. A porous sponge boundary condition is used for the lateral boundaries in this version of the 2DMM, although other versions permit the additional choice of a symmetric or a periodic boundary condition. At the top of the model $\partial\pi/\partial t$ is specified according to an algorithm designed to prevent spurious gravity waves, and at the surface the vertical motion (h in σ_z coordinates) is set at 0.

This version of the 2DMM includes parameterizations of precipitation and cloud physics, and deep cumulus (Cu) convection. The precipitation and microphysics parameterization is based on Kessler,⁸ except that cloud water condensation and evaporation take place "via mutual isobaric adjustment to T , q , and c ." Cu parameterization is called about every tenth time-step, and is essentially a one-dimensional, Lagrangian, sequential plume model which releases potential instability.⁵ Such instability occurs whenever $\partial\sigma/\partial z < 0$ where σ = static energy, and $\sigma = \pi\theta_v + Lq + gz$ where L = latent heat of condensation (or sublimation) and g = gravity. Other versions of the model contain a radiation parameterization, and in the future should include a parameterization of the turbulent boundary layer (more details are found in Loveland*).

⁶C. W. Kreitzberg and D. J. Perkey, 1977, "Release of Potential Instability: Part II. The mechanism of convective/mesoscale interaction," J Atmospheric Sci, 34:1571-1595

⁸E. Kessler, 1969, On the Distribution and Continuity of Water Substance in Atmospheric Circulation, Meteorol Monograph No. 32, American Meteorological Society

⁵C. W. Kreitzberg and D. J. Perkey, 1976, "Release of Potential Instability: Part I. A sequential plume model within a hydrostatic primitive equation model," J Atmospheric Sci, 33:456-475

*K. T. Loveland, 1980, Unpublished manuscripts on the two-dimensional, hydrostatic, primitive equation model, Department of Physics and Atmospheric Sciences, Drexel University, Philadelphia, PA, 238 pp

3. MODEL MODIFICATIONS

Two changes in the program were suggested by Loveland* to make the model more "realistic." One change involved the insertion of certain changes in atmospheric variables caused by Cu convection; the other change involved a better way of computing vertical velocities below, near, and above H (the level at which σ_z heights convert to z). The Cu changes were supplied by Loveland, but the modification of vertical velocity computations required considerable work on our part. The correction of an incorrect sign in the documented equations solved a troublesome computational difficulty and showed that an apparently insignificant mistake in documenting a program can lead to significant errors. A further modification to the program restricted the output to initial values and values between specified times⁹.

Several other relatively minor modifications were made in the program to permit the input of terrain heights on a grid point by grid point basis. In this manner a wedge shaped terrain was inserted such that the terrain rises from one side to the other at a constant slope.

4. RESULTS AND SAMPLE OUTPUT

The output from a series of 20 computer runs is presented in table 1 for a variety of meteorological and geographical conditions. Input parameters were varied, and the results of the computations were compared for seven variables in the vertical column above grid point 11 after 700 minutes of model time unless otherwise noted. The modifications in temperature, relative humidity, and wind apply to the sounding presented in figure 1. The two types of atmospheres (that is, "moist" and "dry") and the flat and mountain terrain types were described in Cogan.⁹ In the "dry" atmosphere the initial specific humidity (q) at all levels is arbitrarily set to 70 percent of the initial specific humidities computed from the input sounding, and no precipitation is allowed to form. The mountain is sinusoidal, with a maximum height of about 1 km at grid point 12, and extends from grid point 6 to 18. The "wedge" terrain is simply an inclined plane slopping upward from west to east (left to right in the relevant figures) and east to west when "reversed." Generally the results follow expected meteorological outcomes, such as greater precipitation and cloud development when the atmosphere is made less stable through the insertion of a sinusoidal mountain or via an increase in temperature at all or at the lowest levels. The most precipitation of all 20 cases occurred when both a sinusoidal mountain was inserted and the temperature of the lowest layers was increased (see case 11 of table 1.) This case had the greatest vertical velocities and least total static energy. An attempt was made to compute a similar example, the same as case 11 except with a dry atmosphere, but the

*K. T. Loveland, 1980, Unpublished manuscripts on the two-dimensional, hydrostatic, primitive equation model, Department of Physics and Atmospheric Sciences, Drexel University, Philadelphia, PA, 238 pp

⁹J. L. Cogan, 1980, Implementation and Analysis of a Mesoscale Moisture Model, Internal Report, US Army Atmospheric Sciences Laboratory, White Sands Missile Range, NM

program would not run more than about 320 minutes of model time using a one-fourth time-step (about 20 seconds) as a consequence of computational instabilities. The program "crashed" even earlier when half and full time-steps were used. Similar computational instabilities arose when the horizontal windspeed (U) was doubled at all levels for the case of the mountain terrain.

In the so-called dry atmosphere, q can change only as a result of temperature changes. Nevertheless, relative humidities of ≥ 100 percent are reached since Cu develop although no precipitation is allowed to form. In the case of a dry atmosphere with the sinusoidal mountain, Cu develop in the 20-minute periods before 680 and 700 minutes, while no clouds occur with the dry flat case. The probable cause of these convective clouds is the enhanced vertical velocity (w) caused by the presence of the mountain which results in greater cooling of the lifted air. Table 1 lists vertical velocities at approximately 1, 4, 7, and 10 km. Nearly all the magnitudes of w ($|w|$) are larger when the mountain is present (for example, compare cases 2 and 4).

The sample runs with the sinusoidal mountain have less precipitable water (PW) and less static energy, except for case 14 which has a "desert" type atmosphere. As one would expect, greater condensation of water vapor to form cloud droplets or precipitation (moist cases only) would tend to decrease the amount of water substance held in the form of vapor. Generally, more clouds formed in the mountain cases for the periods ending at 680 and 700 minutes. Among the first four runs (input values of horizontal wind, temperature, or relative humidity not changed) the moist atmosphere, mountain terrain case with significant precipitation had a lower value of PW at 700 minutes than the dry atmosphere, mountain terrain example. Throughout, the trade-off between static energy and vertical velocity appears to be fairly consistent, high (low) values of static energy go along with low (high) values of w. Since static energy partly consists of potential energy, such a trade-off is not unreasonable ($\sigma = \pi Q_v + Lq + gz$, where gz = potential energy and the other symbols are as defined in section 2). Total releasable instability (TRI) in a column is larger by at least two orders of magnitude for the flat terrain runs at 700 minutes, a result that is not surprising since TRI is released during convection and no Cu develop during the 20-minute period ending at 700 minutes for the flat terrain runs (none in 7 of 10 cases at 680 minutes). Temperatures seem fairly independent of variations in model input parameter at all levels except, of course, when the changed input was T.

The insertion of a wedge terrain generally produced amounts of total PW and precipitation that were between the amounts calculated for the flat and for the mountain cases (compare the relevant cases in table 1). The two exceptions were case 14 where the humidity was arbitrarily decreased in the lower half of the atmosphere and case 17 where the wedge was "reversed." When the initial sounding was "dried out" (relative humidities of 20 percent in the lowest 3 km and 50 percent for the 4 to 8 km layer), the total PW was the lowest for all cases (6.81 cm). This sounding may be considered to crudely represent a cool desert atmosphere such as may be found at White Sands on a cool, dry autumn day. A "reverse" wedge results in a downslope flow at all grid points which would tend to suppress convection and, therefore, precipitation.

In a further comparison using the wedge terrain, the results of running the program with the initial horizontal velocities reversed, that is, $u = -u$ at all levels (case 18), did not coincide with the results where the slope of the wedge was reversed, that is, slope downward to the east (case 17). This outcome could be expected since the model sets up a constant normal velocity (v component) which interacts differently with an east to west wind ($-u$) than with a west to east wind (u). Nevertheless the computed values were similar at 700 minutes except for total precipitation and vertical velocities at levels < 7 km. In addition, the difference in total precipitation diminished considerably at 720 minutes (from 440 to 123 mm). With the flat terrain, increasing the horizontal windspeed throughout the sounding by 2 ms^{-1} or at the 10 and 11 km levels by 5 ms^{-1} , or doubling it at all levels appeared to have little effect on the output relative to that using the "standard" initial atmosphere described in figure 1. The relevant values are given in cases 2, 7, 15, and 16 of table 1. Reducing the horizontal wind to 0.1 ms^{-1} at all levels when using the mountain terrain caused weaker values of w , precipitation, and apparently convection (compare cases 2 and 6).

A final comparison was made between the "original" version of the 2DMM as it arrived at ASL and the revised version currently in use (cases 20 and 4 of table 1). Some of the results indicate more and/or stronger convection for the original version (that is, higher values of precipitation and more clouds built), while others seem to suggest less and/or weaker convection (that is, higher total static energy and more PW*). The apparent paradox of this comparison possibly could be resolved if most of the precipitation fell during the first, say, 6 hours, as suggested by results presented in section 5.2 of this report and if the atmosphere tended to become more stable afterwards. If the precipitation occurred earlier in the "unmodified" program, or the atmosphere stabilized more rapidly after 6 hours, then a higher value of total precipitation could be computed at 700 minutes along with a higher value of, say, total static energy.

5. CROSS-SECTIONAL ANALYSES

To obtain a better idea of the effect of varying the input parameters, and to obtain a two-dimensional view, we constructed cross sections of vertical velocity,** graphs of accumulated precipitation (AP), and graphs of rain rate

*In the context of this report and the 2DMM, convection may be enhanced indirectly as a result of orographic effects via the mescale destabilization of the atmosphere. The relationships of the computed variables to apparent strength and/or amount of convection were suggested by the other comparisons made for this report.

**These are mesoscale values, not the values inside the convective plumes.

(this latter quantity for time variation of results only). All of the cross sections and graphs were derived from computer runs using a moist atmosphere (that is, precipitation allowed to form and initial values of relative humidity not altered). A series of cross sections of vertical velocity*** (w) and graphs of total AP were prepared for runs with different input parameters at the model time of 720 minutes (figures 2 through 7). Another set of cross sections and graphs (figures 8 through 13) include w in cm s^{-1} , AP in millimeters, and precipitation rate (PR) in millimeters per 10^4 seconds for every 2 hours of model time from 120 to 720 minutes for the case of a sinusoidal mountain.

5.1. Variation of Input Parameters at Constant Model Time.

Figure 2a shows the cross section of w , and figure 2b presents the graph of AP for the case with flat terrain. AP does not vary, except near the lateral boundaries (grid points 1, 2, 24, 25); the enhancement at the boundary grid points is probably an artifact of the boundary conditions. A similar enhancement apparently occurs in most of the other cases as well. Figure 2a illustrates the relative lack of activity in the flat terrain case where the magnitude of w is less than 0.1 cm s^{-1} everywhere. A lack of significant convection also is indicated in figure 2b where AP is only about 0.6 mm except near the lateral boundaries.

Values of w and AP showed significant increases when the input parameters were changed for either terrain or temperature. Figures 3a and b show values of the above variables when the lower layers of the atmosphere are heated arbitrarily by 5°C at the surface through 1.0 km, 3°C at 2.0 km, and 1.5°C at 3.0 km. Vertical velocity below 10 km is nearly everywhere negative (downward motion) with values of the largest magnitude to the right of the figure where some exceed -1.5 cm s^{-1} . A band of weak positive w overlies the stronger negative zone from grid point 1 to 23. The orientation of higher values to the right (east) possibly arises from the rightward (eastward) propagation of convection by the mean horizontal flow (u). Part of this larger magnitude may be a result of boundary effects as suggested by figure 3b, where the "true" precipitation amounts are probably represented by those for columns 7 through 20. Values of AP for columns 1 through 6 and 21 through 25 are probably contaminated by boundary effects that have propagated towards the center.

The enhancement by boundary effects also is apparent in figures 4a and b where lower level heating is combined with the inclusion of the sinusoidal mountain. Aside from the boundary enhancement, AP is everywhere greater than for

***Vertical velocity below H , the level (here 3.5 km) which separates terrain following coordinates from ordinary coordinates above, should be strictly denoted as \hat{w} where \hat{h} is height. However, to avoid more complicated cross sections, we follow the convention of the computer output and call all vertical velocities w . For more information on w and \hat{h} , see J. L. Cogan, 1980, Implementation and Analysis of a Mesoscale Moisture Model, Internal Report, US Army Atmospheric Sciences Laboratory, White Sands Missile Range, NM (reference 9), and K. T. Loveland 1980, Unpublished manuscripts on the two-dimensional, hydrostatic, primitive equation model, Department of Physics and Atmospheric Sciences, Drexel University, Philadelphia, PA, 238 pp

the mountain case without the heating (see figure 13b), and the magnitudes of w generally are larger by a factor of two or more (compare figure 4a with figure 13a). The mean value of AP and most individual values of magnitude of w ($|w|$) are larger than the respective values computed for the case of flat terrain with lower level heating (figures 3a and b). Furthermore, figures 4a and b suggest a more organized convection, especially on the windward (west) side of the mountain where there is a zone of high AP centered on grid point 8. The case presented in figures 4a and b produces the most convection and seems to be the least stable of the successful computer runs to date. When surface heating and the sinusoidal mountain were added to a "dry" atmosphere, the program aborted after about 320 minutes of model time even with a reduced time-step. Perhaps boundary instabilities propagated to the center and beyond, reinforced one another, and overwhelmed the smoothing routines. In the moist case, some energy was diverted to precipitation, but not in the "dry" case. This diversion may have reduced other variables such as w sufficiently so that extreme values were avoided.

Figures 5a and b show the output where the terrain is in the form of a wedge as an inclined plane sloping from left to right (west to east). Here values of w are greater than those for the flat terrain, but significantly less than in most other cases (compare figures 2a, 3a, 4a, 5a, and 13a). The positive and negative regions of w are organized primarily in the horizontal with a ribbon of positive w overlying a band of negative w . Figure 5b shows that overall precipitation was nearly as great as with the sinusoidal mountain (about 59.5 versus 62 mm), but that no obvious boundary enhancement and no peak zone occurred (compare with figure 13b). The precipitation in the wedge terrain case is more uniformly distributed even though more precipitation falls on the windward (left) part of the wedge. This decrease in AP from west to east suggests that the atmosphere is progressively "dried out" in the downwind direction.

A comparison also was made between the results of the unmodified "original" version of the 2DMM (figures 6a and b) and the version modified by the author (figures 13a and b). The sinusoidal mountain terrain was used with the "standard" atmosphere of figure 1 because it was expected that this case would show any significant differences without causing numerical instabilities and a program abort. In figure 6a the zones of w are more horizontal than in figure 13a, with an area of negative w over the mountain surmounted by alternating layers of positive and negative values. The locus of maximum values of w roughly runs from about 1 km over the top of the mountain at grid point 13 to about 8 km near grid point 17 and appears to extend up through a relatively weak zone of positive w to around grid point 18 or 19 near the "top" of the atmosphere at 14 km. The cross section of w from the modified 2DMM (figure 13a) shows more organization with alternating plumes of positive and negative w . As in figure 6a, an area of negative w lies over the mountain at grid point 13, but the remainder of the pattern is quite different. Maximum values of $|w|$ are similar, but the locus of the maxima is nearly horizontal. The graph of AP for the unmodified program (figure 6b) is sharply peaked about grid point 9, with a maximum value more than twice the maximum for the modified program (figure 13b). However, outside the zone of heavy precipitation amounts between grid points 6 and 12 (the entire windward side of the mountain), the modified program generally produces higher values. If the peak centered on grid point 9 were removed, figure 6b would closely resemble figure 2b for flat terrain. The modifications to the 2DMM apparently caused less

instability and convection in the peak zone but more over the other grid points. The changes also seem to affect the distribution of w more than its magnitude.

Several other graphs of AP were prepared for three computer runs using the wedge terrain. Figure 7a shows the result on AP of a wedge of half the slope as that for figure 5b. The total amount of precipitation is reduced by about one-third, and AP only slightly decreases downwind to the right (east). The grid point to grid point variation in AP increased somewhat, and once again boundary effects are not obvious. Nevertheless, the reduced wedge still produces more than twice the total AP of the flat terrain case. Two further computer runs (figures 7b and c) indicate that little difference in AP arises when u is reversed (that is, $u = -u$) as compared with reversing the wedge (that is, upward sloping to the left [west]). The total amounts of AP are nearly the same (20.286 and 19.689 mm, respectively), and both cases produce only slightly more precipitation than the flat terrain case (17.430 mm). In figure 7b the boundary appears to affect the rightmost grid points and in figure 7c the leftmost grid points. For these latter runs the half-magnitude wedge was used; a larger wedge may have resulted in relatively more significant differences in AP.

5.2. Time Variation of Results

A series of computer runs was performed to obtain a set of cross sections and graphs every 2 hours of model time for w , AP, and PR. Precipitation mostly arises from convective processes, but occasionally there is a contribution from so-called "stable" processes. In the context of the 2DMM, "stable" precipitation arises from mesoscale uplift (the values of w shown in the cross sections of this paper). PR arising from "stable" precipitation is labelled whenever it occurs. Otherwise precipitation is assumed to be of the convective type. Note that AP may consist partly of stable precipitation, but it was not separated out in the respective graphs because of the extremely small amounts involved. For example, the greatest absolute and proportional amount of stable AP was computed for the sinusoidal mountain case where 0.193 mm occurred out of a total AP of 62.064 mm or 0.31 percent. Figures 8 through 13 show the changes that took place in the field of w and in AP and PR amounts as a function of time. PR is the rate at the indicated time; other values may occur at other times.

The cross sections of w show that its magnitude did not change significantly until sometime between 480 and 600 minutes (compare figures 11a and 12a), but that the sign and organization of w showed some important changes beginning after the initial output at 120 minutes. Over the center of the mountain near grid point 13 at heights around 3 to 5 km, a region of relatively strong negative w at 120 minutes weakened and became a region of positive w of about the same magnitude at 360 minutes. At 480 minutes that same region contained somewhat weaker negative values; at 720 minutes these negative values had strengthened considerably. During the 12 hours of model time, the orientation or slope of the major regions of positive and negative w reversed direction. Regions of w generally sloped upward from right to left (east to west) at 120 minutes, becoming nearly horizontal at 360 minutes. The horizontal stratification began to break down by 480 minutes and was replaced by a generally vertical orientation at 600 minutes. By 720 minutes, the pattern of w sloped upward from left to right (west to east).

The graphs of AP indicate that most of the precipitation in the peak region (that is, grid points 6 through 12) occurred during the first 240 minutes. Important amounts of precipitation did not develop outside the peak region until around 480 minutes. These observations are supported by the figures of PR plotted against distance in kilometers or grid point. Virtually no precipitation took place at 360 minutes when the zones of w were nearly horizontal. Stable precipitation first appeared on the graphs of PR at 480 minutes (figure 11c) although the computer output indicated that some stable precipitation occurred between 240 and 360 minutes. All of the stable precipitation occurred over grid point 12 throughout the entire 12-hour model period.

Apparently the upslope flow over the mountain stimulates the development of convection and the generation of stable precipitation. The b and c parts of figures 8 through 13 relate AP and stable PR to the location of the mountain as indicated by the double-headed arrow on each graph. The size and shape of the mountain are indicated on each of the cross sections. After the atmosphere "drys out" in the peak zone, convection forms downstream, increasing AP at most grid points > 12.

6. SUGGESTIONS AND CONCLUSION

The results of computations using the 2DMM have a positive potential to provide some useful input for some EO algorithms. As an example of a possible use of output from the 2DMM, we refer to section 2.2 on "Natural Aerosols" of Duncan et al.⁷ The algorithm used in this section has the form of $y = cx^b$, where $c = 10^a$, y is the extinction coefficient in the desired spectral band, x is the coefficient for visible radiation, and a and b are constants extracted from empirical data for various atmospheric situations. Here x is derived from Koshmeider's relation, $x = 3.912/V$ where V is visibility. The constants a and b are assumed to be valid for all types and intensities of rain. However, this assumption may be an oversimplification even though visibility is crudely related to quantities such as PR. Perhaps a better algorithm would be one that uses PR directly as input.* Computed results from the 2DMM could provide the input for a relationship between PR and attenuation such as those presented by Chen¹⁰ in his figures 3 and 4 and his table 1.

Suppose that we have two rainfall situations that produce similar visibilities but different PR. A light rain with many small drops may result in the same

⁷L. D. Duncan et al, 1979, The Electro-Optical System Atmospheric Effects Library, Volume I, Technical Documentation. ASL-TR-0047, US Army Atmospheric Sciences Laboratory, White Sands Missile Range, NM

*The latest version of EOSAEL to be called EOSAEL 80 will use an algorithm that computes the extinction coefficient for rain as a simple function of rain rate. This change is a step towards a more realistic representation of extinction by "natural aerosols."

¹⁰C. C. Chen, 1975, Attenuation of Electromagnetic Radiation by Haze, Fog, Clouds, and Rain, Report No. R-1694-PR, Rand Corporation, prepared for the US Air Force under contract F44620-73-C-0011, Santa Monica, CA

visibility as a heavier rain with fewer but much larger drops. The algorithm presented by Duncan et al would compute one value of the extinction coefficient for the, say, 3 μ m to 5 μ m infrared. However, using PR and figure 3 of Chen we would obtain two values. For example, doubling the PR from 4 to 8 mm per hour would increase the extinction coefficient from about 2.5 to about 4.2 dB km⁻¹. Such values of PR are not unreasonable. The significance of better estimates of the extinction coefficient depends on the characteristics of the particular sensors.

Duncan et al⁷ as well as the author of this report recognize that the present empirical extinction models are far from the best possible algorithms for the estimation of attenuation by so-called natural aerosols. Duncan et al note "Until techniques are developed to predict composition and size distribution from meteorological measurements, a model which does not depend on aerosol microphysical data must be adopted."⁷ However, a more realistic 3DMM of the type described by Cionco² and Kreitzberg et al¹ could provide useful input, for example, in the form of drop-size distributions within specified fogs or rain types. The need for field experiments would be reduced to the few needed for "calibration" and verification of a 3DMM. A 3DMM then could provide data for EO algorithms for a large variety of atmospheric conditions and terrain types.

The sensitivity analysis performed for this report indicated the large amount of information on mesoscale moisture processes available from the relatively uncomplicated 2DMM. A limitation of the model was the inability to avoid computational instabilities for the combination of an unstable sounding and sizable variations in terrain. The insertion of relatively small terrain features stimulated large changes in precipitation amount and vertical velocity. The large differences in precipitation amount are supported at least qualitatively by common observations, for example, more rain in mountainous areas and where there is upslope flow. Work with the 2DMM suggested that placement of a field experiment in an unrepresentative location could result in misleading data. Also data taken in a so-called representative location under "typical" meteorological conditions may lead to unreliable results if there are significant variations in terrain and/or atmospheric conditions within the area of concern. For example, a significant deviation from "typical" values of temperature of the lower atmosphere leading to a large change in convection and a consequent increase in precipitation rate, is likely to cause serious problems for the application of EO algorithms if such variations

⁷L. D. Duncan, 1979, The Electro-Optical System Atmospheric Effects Library, Volume I, Technical Documentation. ASL-TR-0047, US Army Atmospheric Sciences Laboratory, White Sands Missile Range, NM

²R. M. Cionco, 1980, Moisture Analysis, Depiction and Prediction System of Models: Description of the ASL Program, Internal Report, US Army Atmospheric Sciences Laboratory, White Sands Missile Range, NM

¹C. W. Kreitzberg, W. D. Mount, and B. R. Fow, 1979, Preliminary Evaluation of Meteorological Models for Moisture Depiction and Prediction for Electro-Optical Applications, Contract DAAG29-76-D-0100, US Army Research Office, PO Box 12211, Research Triangle Park, NC

were not considered during planning of the experiment. Additionally, climatological values of meteorological variables may be misleading if applied to a location where meteorological conditions fluctuate widely or the terrain varies greatly. Consequently, the results of computations using the 2DMM should provide useful information for those developing and applying EO algorithms. A more complex 3DMM can produce input for improved EO algorithms in the form of composition and size distribution of microphysical parameters.

TABLE 1. VALUES OF SEVEN VARIABLES COMPUTED BY THE 20MN FOR TWENTY SETS OF MODEL INPUT PARAMETERS*

Model Input Parameters	Total Precipitation (mm)	Number of Clouds Built in all Columns at t = 700 and 680	Total Static Energy (Jg ⁻¹)	Total PH (cm)	TBL (m ² s ⁻²)	W (or h) at 1, 4, 7 and 10 km (cm s ⁻¹)	T at 1, 4, 7, and 10 km (°C)
(1) Flat terrain, dry	0.0	0 (700) 0 (680)	3031.9	24.86	452.5	-0.011 -0.039 +0.002 +0.024	9.3 -10.7 -30.9 -50.3
(2) Flat terrain, moist	0.623	0	3030.0	24.41	315.3	-0.007 -0.020 +0.011 +0.025	9.2 -10.8 -31.0 -50.3
(3) Sinusoidal mountain, dry	0.0	3	2733.6	15.96	1.7	-0.119 -0.746 +0.212 +0.190	8.4 -10.9 -30.6 -51.0
(4) Sinusoidal mountain, moist	3.664	0 4	2728.3	13.71	0.0	-0.092 -0.967 +0.470 +0.374	8.4 -10.6 -30.4 -50.9
(5) Flat terrain, dry U = ux2	0.0	0 0	3029.2	24.85	458.6	-0.015 -0.043 -0.012 +0.022	9.2 -10.7 -31.0 -50.4
(6) Sinusoidal mountain, moist U = 0.1 ms ⁻¹ (0 at surface)	0.275	1 1	2735.4	15.50	0.0	-0.002 -0.066 +0.040 +0.051	9.0 -10.4 -31.0 -50.6
(7) Flat terrain, moist U = ux2	0.623	0 0	3031.9	24.42	309.0	-0.006 -0.017 +0.001 +0.013	9.2 -10.7 -31.0 -50.4
(8) Sinusoidal mountain, moist T = T + 5°C	9.509	2 2	2775.7	18.20	0	-0.079 -0.789 +0.408 +0.481	13.8 -4.7 -23.7 -45.4
(9) Flat terrain, moist T = T + 5°C	2.708	0 2	3082.5	31.59	0	-0.067 -0.192 -0.105 +0.030	14.7 -4.3 -23.9 -45.2
(10) Flat terrain, moist 0-1 km T = T + 5°C 2 km T = T + 3°C 3 km T = T + 1.5°C	6.193	0 2	3019.5	24.24	1646.9 (0 at 680 min)	-0.235 -0.741 -0.652 -0.210	13.2 -5.9 -26.8 -50.6

TABLE 1. (cont)

Model Input Parameters	Total Precipitation (mm)	Number of Clouds Built in all Columns at t = 700 and 680	Total Static Energy (Jg ⁻¹)	Total PM (cm)	TR1 (m ² s ⁻²)	W (or h) at 1, 4, 7 and 10 km (cm s ⁻¹)	T at 1, 4, 7, and 10 km (°C)
(11) Sinusoidal mountain, moist 0-1 km T = T + 5°C 2 km T = T + 3°C 3 km T = T + 1.5°C	9.737	11 7	2700.4	15.10	213.4	-0.137 -2.978 -2.534 -0.250	11.4 -5.8 -2.0 -41.9
(12) Flat terrain, dry 0-1 km T = T + 5°C 2 km T = T + 3°C 3 km T = T + 1.5°C	0.0	0 2	3034.3	30.43	0	-0.265 -0.573 +0.009 +0.805	15.7 -0.2 -24.5 -50.8
(13) Wedge terrain, moist 0.0-0.48 km	1.629	0 0	2961.4	21.77	0	-0.015 -0.034 +0.029 +0.068	9.5 -10.5 -31.0 -50.2
(14) Flat terrain, moist 0-3 km RH = 20% 4-8 km RH = 50%	0.0	0 0	2984.9	6.81	0	+0.592 +0.722 +0.722 +0.722	8.1 -11.3 -31.0 -50.3
(15) Flat terrain moist 10-11 km U = U + 5 ms ⁻¹	0.623	0 0	3031.7	24.45	317.0	-0.014 -0.031 -0.066 -0.063	9.2 -10.8 -30.9 -40.2
(16) Flat terrain, moist 1-14 km U = U + 2 ms ⁻¹	0.623	0 0	3031.3	24.44	311.5	+0.000 -0.010 +0.017 +0.050	9.2 -10.7 -31.0 -50.4
(17) Wedge terrain, moist 0.48 - 0.0 km	0.384 (0.701 at 720 min)	3 2	2939.6	21.75	685.3	-0.068 -0.229 -0.128 +0.023	9.2 -10.8 -30.8 -50.2
(18) Wedge terrain, moist 0.0 - 0.48 km W = -U	0.824 (0.824 at 720 min)	3 3	2965.2	22.39	726.5	-0.026 -0.051 -0.021 +0.021	9.2 -10.8 -31.0 -50.3
(19) Wedge terrain, moist 0.0 - 0.48 km	0.905	0 0	2996.0	23.03	0	+0.012 +0.031 +0.061 +0.051	9.4 -10.5 -31.0 -50.3
(20) Sinusoidal mountain moist (Unmodified version)	8.669 (8.763 at 720 min)	2 4	2767.1	16.82	253.1	-0.031 -0.575 +0.072 +0.621	9.8 -8.5 -30.2 -51.2

*The values are for column 11 (near the center) and 700 minutes of model time unless otherwise specified. T = temperature, W = vertical velocity, PM = precipitable water, U = horizontal wind, and TR1 = total releasable instability. Total precipitation includes convective and stable types. Initial values of T and W are given in Figure 1 unless otherwise stated.

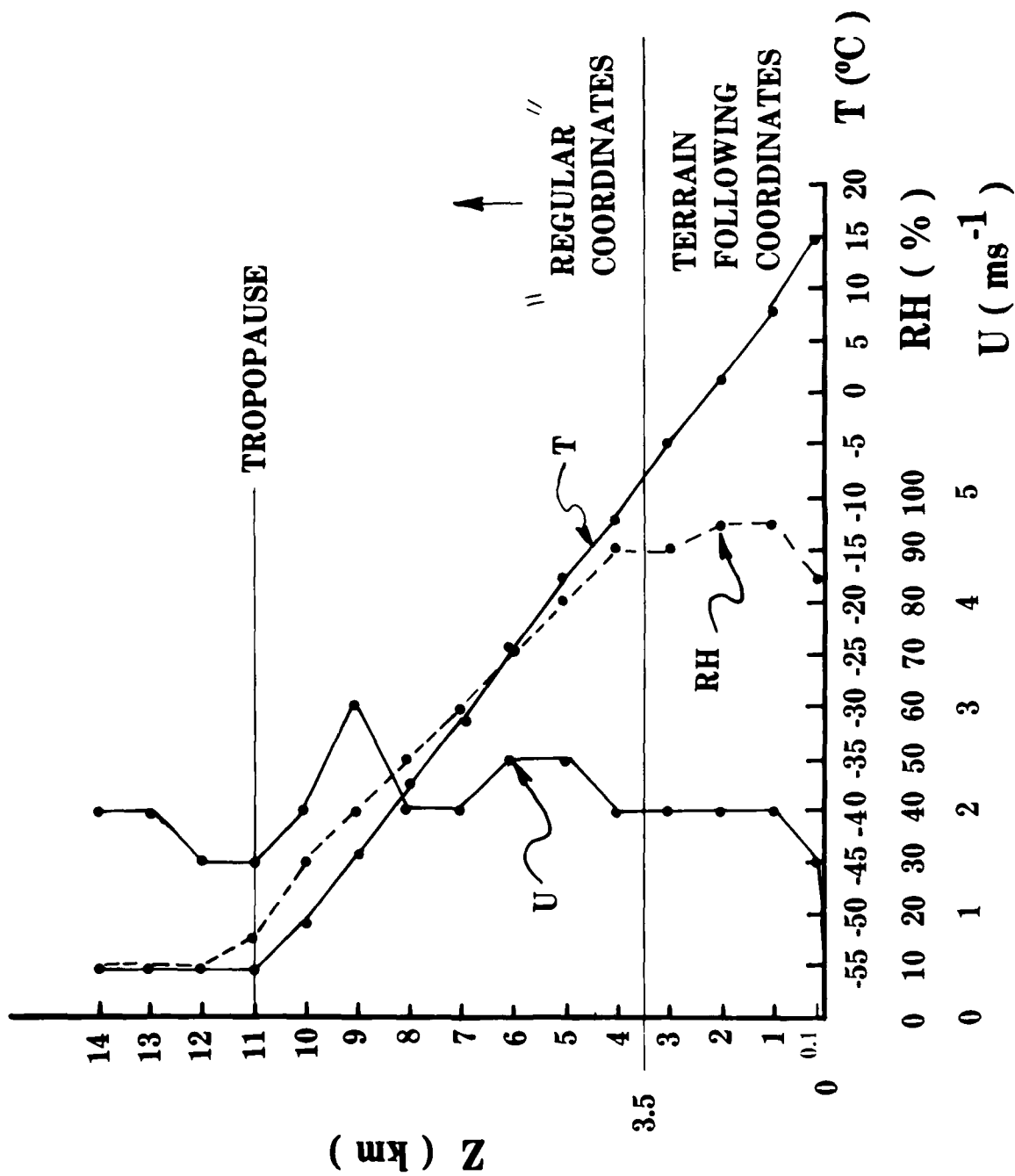


Figure 1. Sounding values for input into the 2DMM. Z is height, T is temperature, RH is relative humidity, and U is the east-west component of wind where positive flow is from west to east.

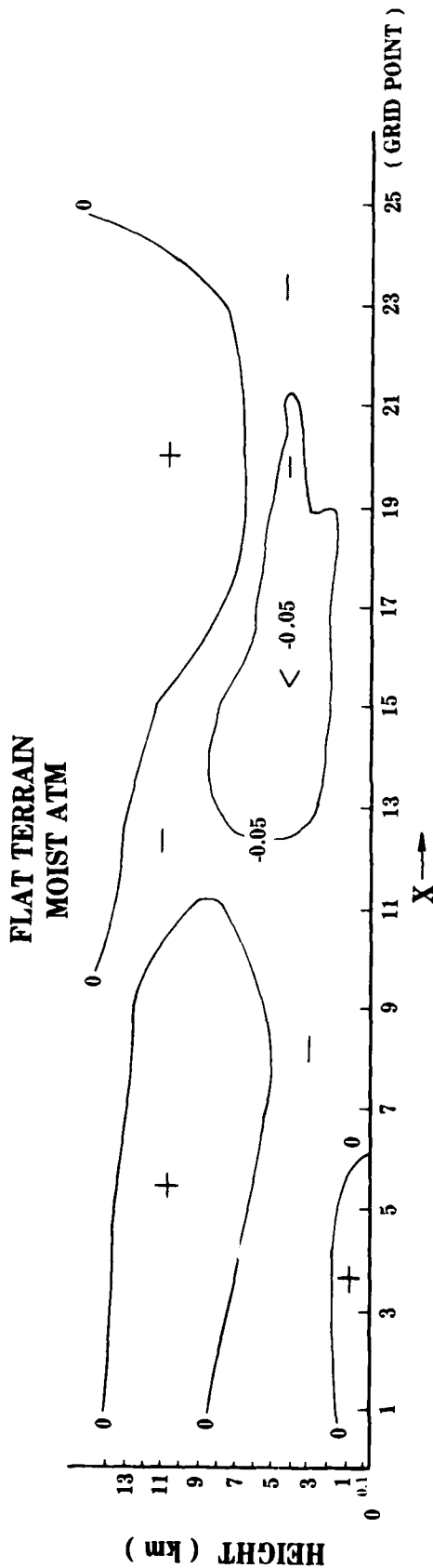


Figure 2a. Cross section of vertical velocity (w) with coordinates of height and horizontal distance (x) for the case of flat terrain and a moist atmosphere (see figure 1) at 720 minutes. Data are plotted for every odd grid point at 16 vertical levels. W is in cm s⁻¹.

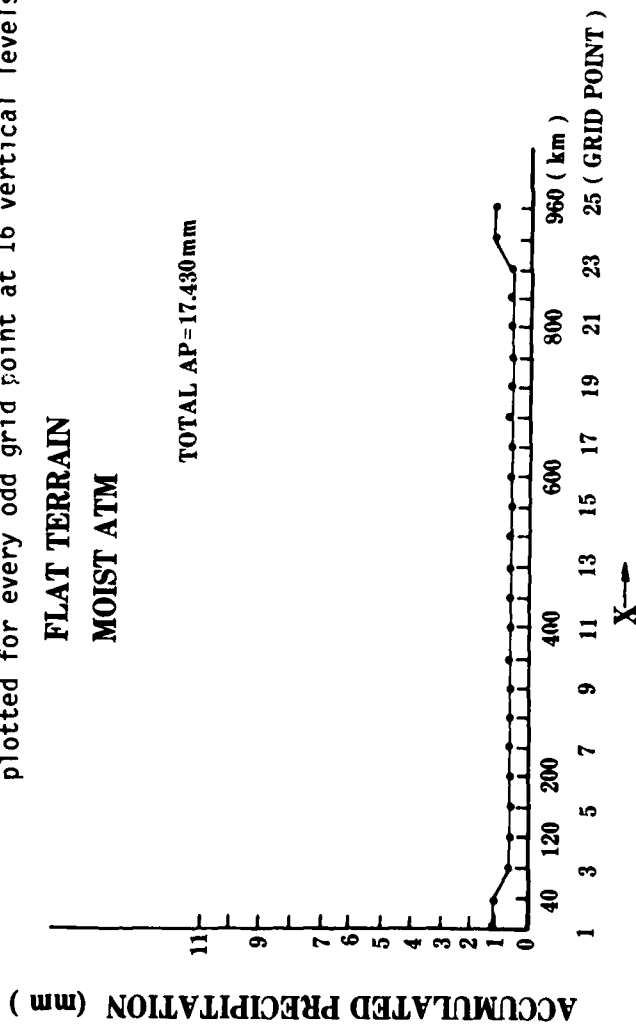


Figure 2b. Graph of accumulated precipitation (AP) plotted against horizontal distance (x) for the moist atmosphere and flat terrain. Total AP is the sum of all grid point values.

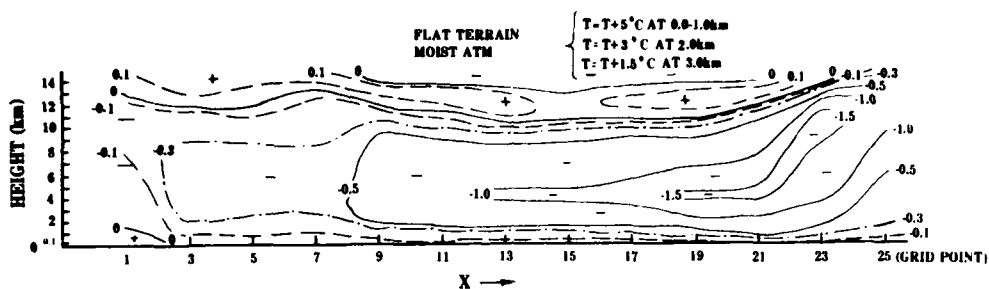


Figure 3a. Cross section of vertical velocity (w) with coordinates of height and horizontal distance (x). The same as 2a except that the temperature (T) sounding was modified so that $T = T + 5^\circ\text{C}$ at 0-1 km, $T = T + 3^\circ\text{C}$ at 2 km, and $T = T + 1.5^\circ\text{C}$ at 3 km.

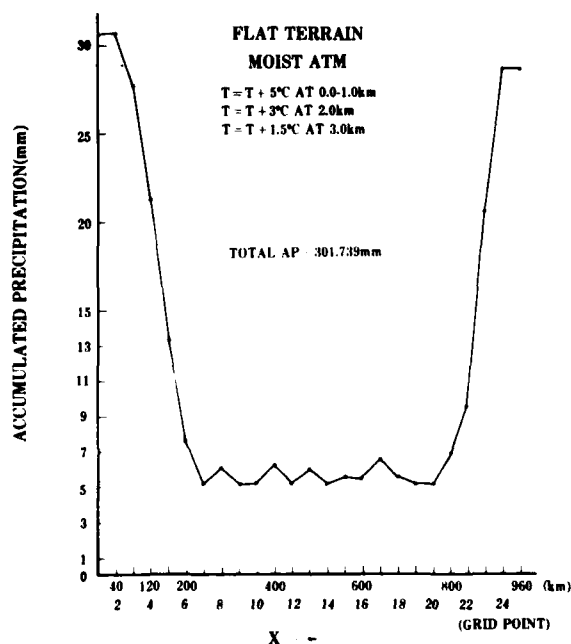


Figure 3b. Same as figure 2b but with the initial vertical profile of temperature (T) modified so that $T = T + 5^\circ\text{C}$ at 0-1 km, $T = T + 3^\circ\text{C}$ at 2 km, and $T = T + 1.5^\circ\text{C}$ at 3 km.

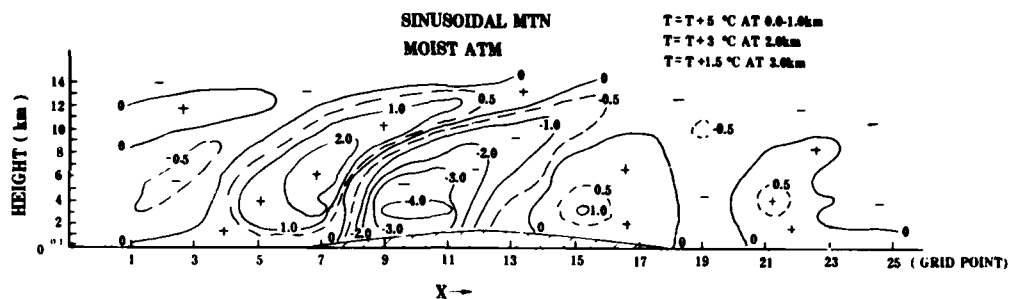


Figure 4a. Cross section of vertical velocity (w) with coordinates of height and distance (x). The same as 2a except that sinusoidal mountain terrain was used (indicated on the cross section) and the initial temperature sounding was modified as for 2b (and indicated on the cross section).

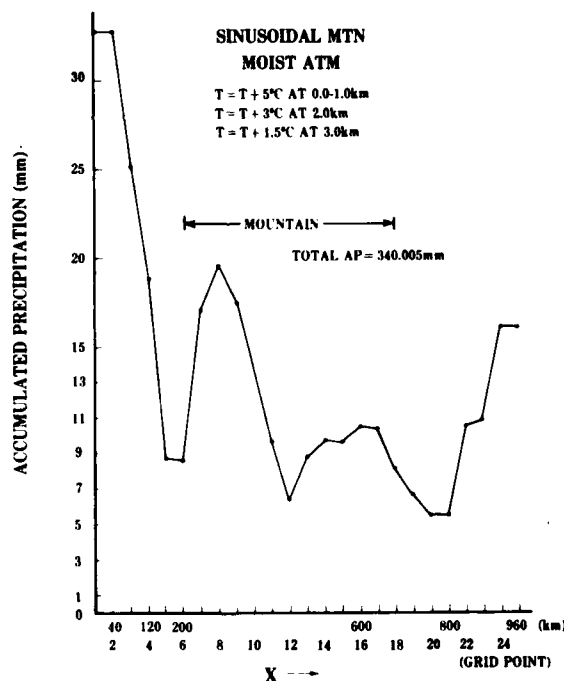


Figure 4b. Same as figure 2b but with the sinusoidal mountain and the initial vertical profile of temperature (T) modified as in 3b. The location of the sinusoidal mountain is indicated by the double ended arrow.

WEDGE TERRAIN (0.0 → 0.96 km)
MOIST ATM

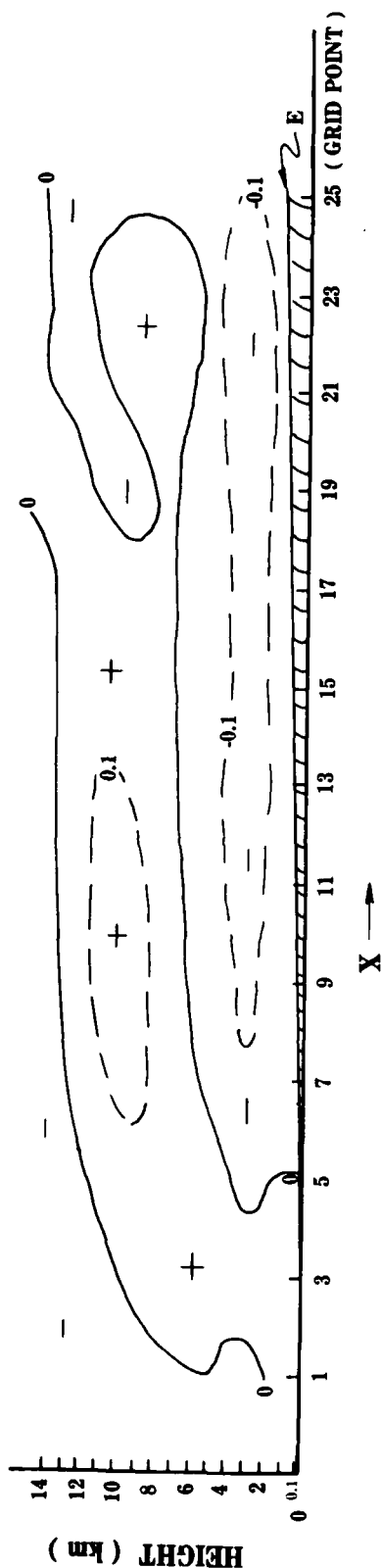


Figure 5a. Cross section of vertical velocity (w) with coordinates of height and horizontal distance (x). The same as 2a except that wedge terrain was used (maximum height of terrain is 0.96 km at grid point 25).

WEDGE TERRAIN (0.0 → 0.96 km)
MOIST ATMOSPHERE

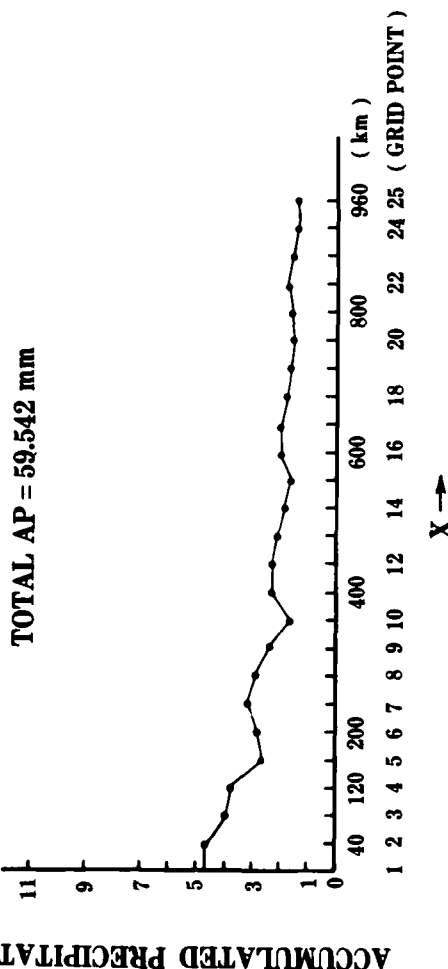


Figure 5b. Same as figure 2b but with wedge terrain (maximum height of terrain is 0.96 km at grid point 25).

The graph displays accumulated precipitation (mm) on the y-axis (0 to 21) against distance (km) on the x-axis (0 to 960). Three models are compared: Sinusoidal MTN (solid line), Moist ATM (line with dots), and UN-Modified Version (line with crosses). A mountain profile is shown as a horizontal line at 11 mm precipitation between 200 km and 400 km. The total precipitation is 86.717 mm.

Distance (km)	Sinusoidal MTN (mm)	Moist ATM (mm)	UN-Modified Version (mm)
0	0.5	0.5	0.5
40	0.5	0.5	0.5
80	0.5	0.5	0.5
120	0.5	0.5	0.5
160	0.5	0.5	0.5
200	0.5	0.5	0.5
240	0.5	0.5	0.5
280	0.5	0.5	0.5
320	0.5	0.5	0.5
360	0.5	0.5	0.5
400	0.5	0.5	0.5
440	0.5	0.5	0.5
480	0.5	0.5	0.5
520	0.5	0.5	0.5
560	0.5	0.5	0.5
600	0.5	0.5	0.5
640	0.5	0.5	0.5
680	0.5	0.5	0.5
720	0.5	0.5	0.5
760	0.5	0.5	0.5
800	0.5	0.5	0.5
840	0.5	0.5	0.5
880	0.5	0.5	0.5
920	0.5	0.5	0.5
960	0.5	0.5	0.5

27

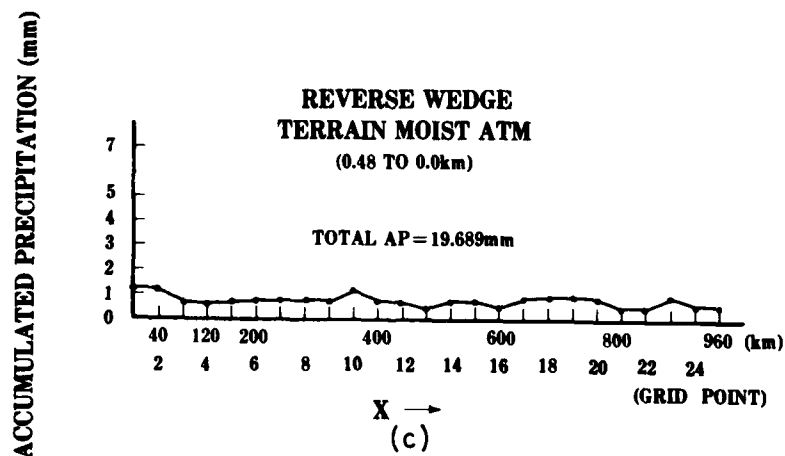
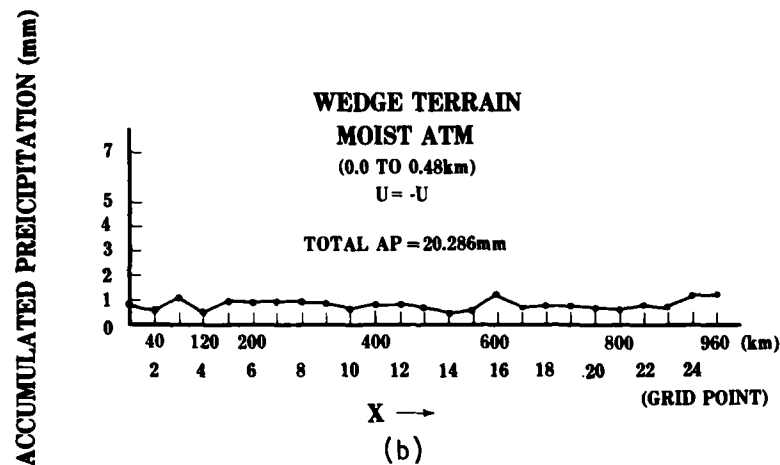
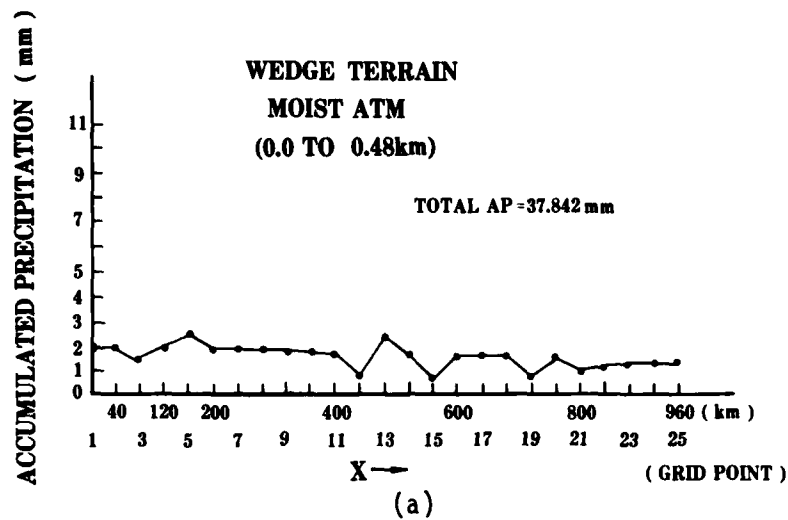
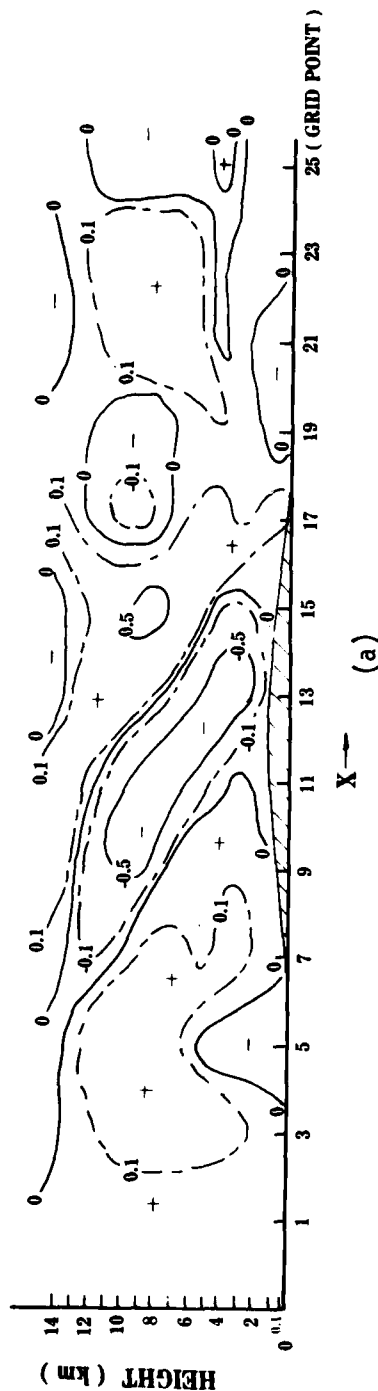


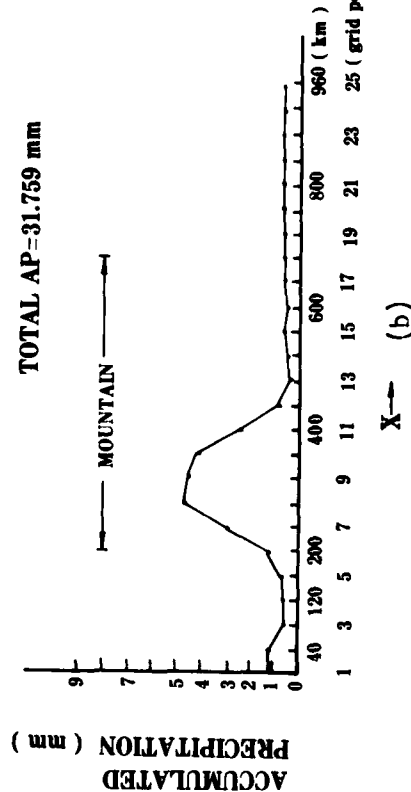
Figure 7. Graphs of accumulated precipitation (AP) plotted against horizontal distance (x). Model input parameters are listed on the separate graphs. Total AP is the sum of all grid point values.

SINUSOIDAL MTN
MOIST ATM



SINUSOIDAL MTN
MOIST ATM

TOTAL AP=31.759 mm



SINUSOIDAL MTN
MOIST ATM

PRECIPITATION RATE
(mm/10⁴s)

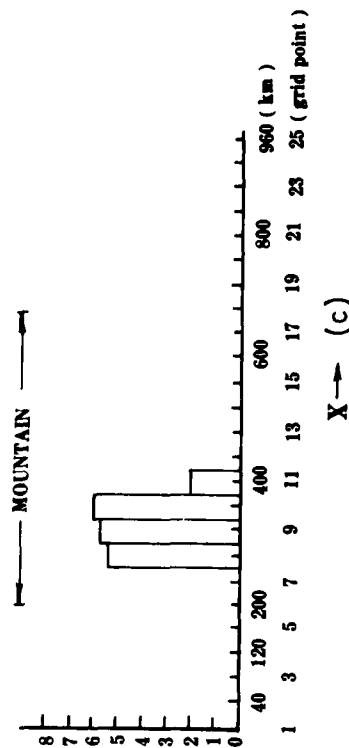


Figure 8. Cross section of vertical velocity (w) with coordinates of height and horizontal distance (x), and graphs of accumulated precipitation (AP) and precipitation rate (PR), using the input parameters of the sinusoidal mountain and a moist atmosphere (see figure 1) at 120 minutes. The cross hatched area on the cross section (a) and the double ended arrow on the graphs (b, c) indicate the location of the mountain. W is in cm s^{-1} . Total AP is the sum of all the grid point values. Horizontal distance is in km and grid point.

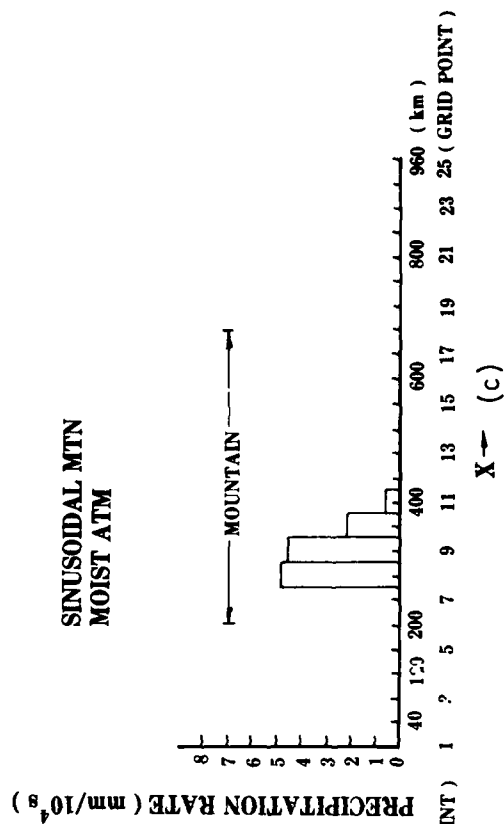
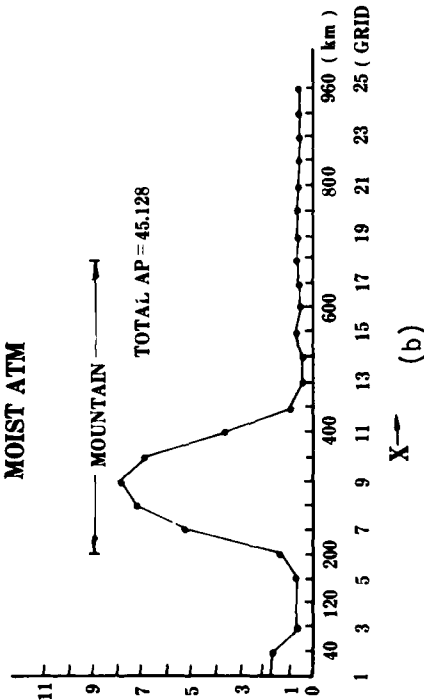
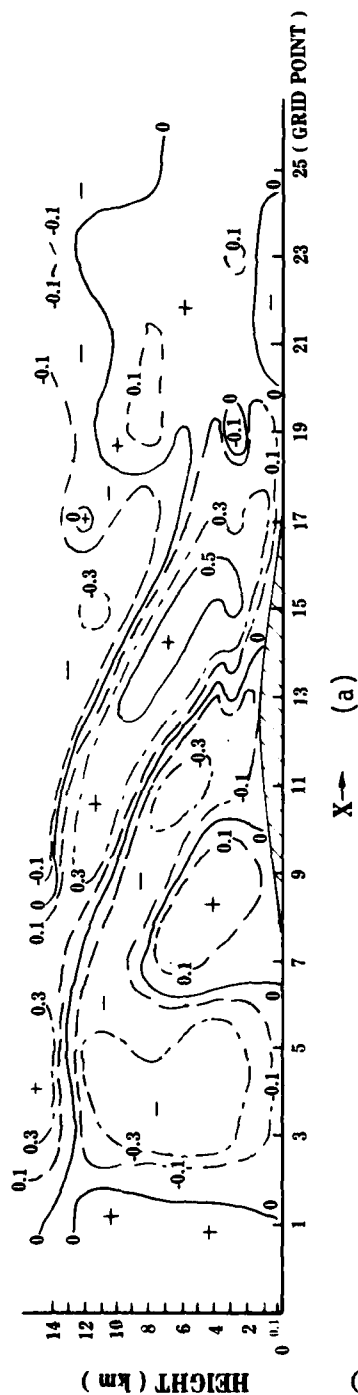


Figure 9. (a) Cross section of vertical velocity (w) with coordinates of height and horizontal distance (x), and (b, c) graphs of accumulated precipitation (AP) and precipitation rate (PR). The same as figure 8 but for 240 minutes.

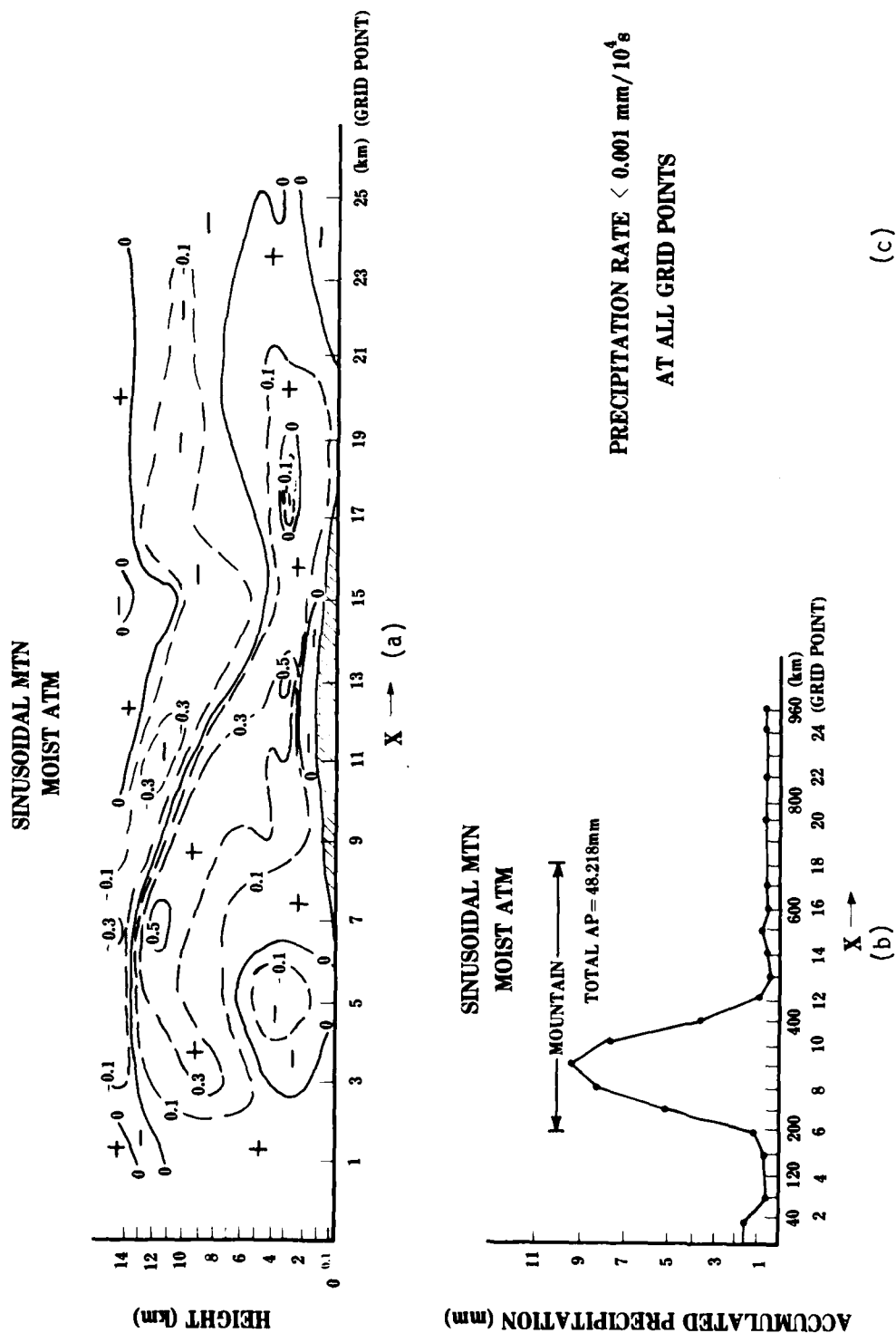
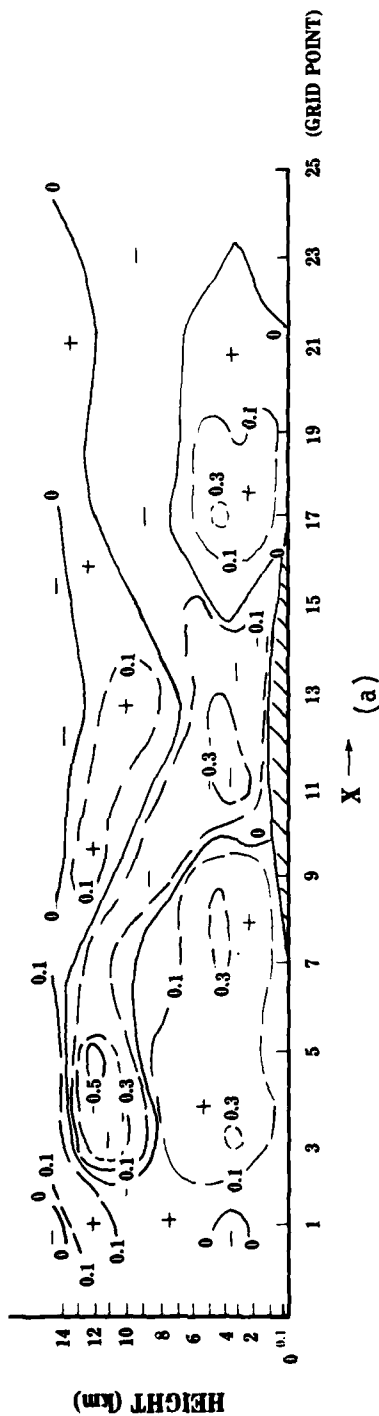
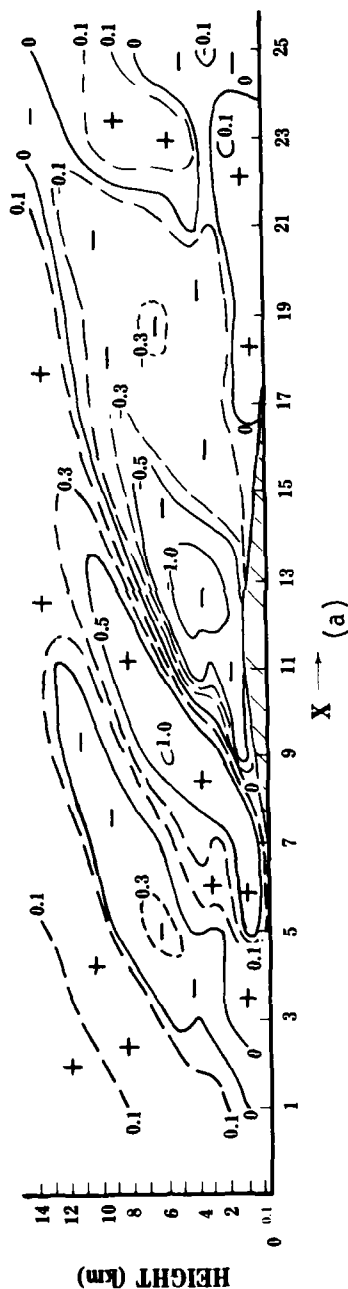


Figure 10. (a) Cross section of vertical velocity (w) with coordinates of height and distance horizontal (x), and (b, c) graphs of accumulated precipitation (AP) and precipitation rate (PR). The same as figure 8 but for 360 minutes.

SINUSOIDAL MTN MOIST ATM



SINUSOIDAL MTN MOIST ATM



SINUSOIDAL MTN MOIST ATM

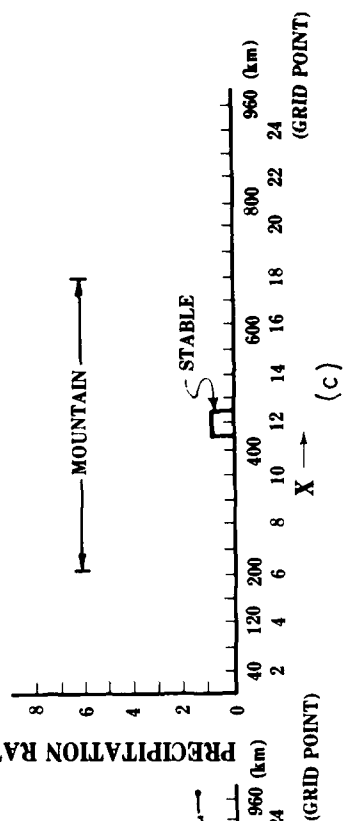
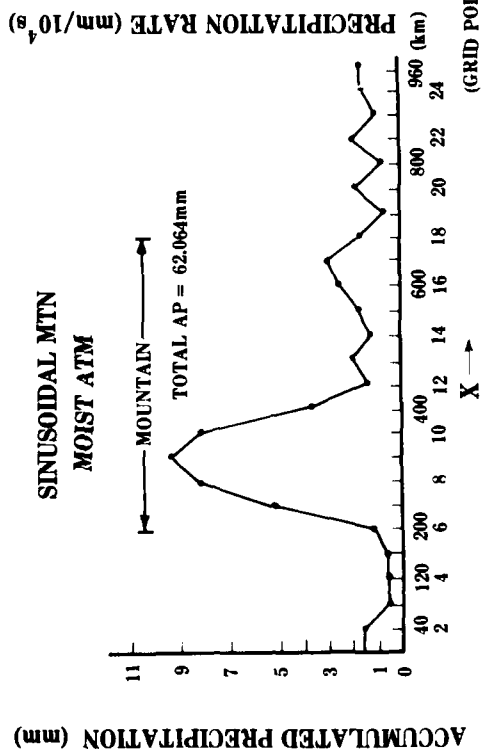


Figure 13. (a) Cross section of vertical velocity (w) with coordinates of height and horizontal distance (x), and (b, c) graphs of accumulated precipitation (AP) and precipitation rate (PR). The same as figure 8 but for 720 minutes.

REFERENCES

1. Kreitzberg, C. W., W. D. Mount, and B. R. Fow, 1979, Preliminary Evaluation of Meteorological Models for Moisture Depiction and Prediction for Electro-Optical Applications, Contract DAAG29-76-D-0100, US Army Research Office, PO Box 12211, Research Triangle Park, NC.
2. Cionco, R. M., 1980, Moisture Analysis, Depiction and Prediction System of Models: Description of the ASL Program, Internal Report, US Army Atmospheric Sciences Laboratory, White Sands Missile Range, NM.
3. Kreitzberg, C. W., D. J. Perkey, and J. E. Pinkerton, 1974, Mesoscale Modeling, Forecasting, and Remote Sensing Research, Project THEMIS Final Report, AFCRL-TR-74-0253, Department of Physics and Atmospheric Sciences, Drexel University, Philadelphia, PA. AD 784875
4. Perkey, D. J. 1976, "A Description of Preliminary Results from a Fine-Mesh Model for Forecasting Quantitative Precipitation," Monthly Weather Rev., 104:1513-1525.
5. Kreitzberg, C. W., and D. J. Perkey, 1976, "Release of Potential Instability: Part I. A sequential plume model within a hydrostatic primitive equation model," J Atmospheric Sci., 33:456-475.
6. Kreitzberg, C. W., and D. J. Perkey, 1977, "Release of Potential Instability: Part II. The mechanism of convective/mesoscale interaction," J Atmospheric Sci., 34:1571-1595.
7. Duncan, L. D., et al, 1979, The Electro-Optical Systems Atmospheric Effects Library, Volume I, Technical Documentation, ASL-TR-0047, US Army Atmospheric Sciences Laboratory, White Sands Missile Range, NM.
8. Kessler, E., 1969, "On the Distribution and Continuity of Water Substance in Atmospheric Circulation," Meteorol Monograph No. 32, American Meteorological Society.
9. Cogan, J. L., 1980, Implementation and Analysis of a Mesoscale Moisture Model, Internal Report, US Army Atmospheric Sciences Laboratory, White Sands Missile Range, NM.
10. Chen, C. C., 1975, Attenuation of Electromagnetic Radiation by Haze, Fog, Clouds, and Rain, Report No. R-1694-PR, Rand Corporation, prepared for the US Air Force under contract F44620-73-C-0011, Santa Monica, CA.

APPENDIX
PROGNOSTIC EQUATIONS

East wind velocity, u

$$\frac{\partial u}{\partial t} = -u \frac{\partial u}{\partial x} - h \frac{\partial u}{\partial h} + fv - \theta_v \frac{\partial \pi}{\partial x} - g\beta \frac{\partial E}{\partial x} + \left(\frac{\partial u}{\partial t}\right)_{cum}$$

North wind velocity, v

$$\frac{\partial v}{\partial t} = -u \frac{\partial v}{\partial x} - h \frac{\partial v}{\partial h} - fu - \theta_v \frac{\partial \pi}{\partial y} - g\beta \frac{\partial E}{\partial y} + \left(\frac{\partial v}{\partial t}\right)_{cum}$$

Virtual potential temperature, θ_v

$$\frac{\partial \theta_v}{\partial t} = -u \frac{\partial \theta_v}{\partial x} - h \frac{\partial \theta_v}{\partial h} + \left(\frac{d\theta_v}{dt}\right)_\mu + \frac{C_p}{\pi} \left(\frac{\partial T}{\partial t}\right)_{cum}$$

Specific humidity, q

$$\frac{\partial q}{\partial t} = -u \frac{\partial q}{\partial x} - h \frac{\partial q}{\partial h} + \left(\frac{dq}{dt}\right)_\mu + \left(\frac{\partial q}{\partial t}\right)_{cum}$$

Cloud water concentration, c

$$\frac{\partial c}{\partial t} = -u \frac{\partial c}{\partial x} - h \frac{\partial c}{\partial h} + \left(\frac{dc}{dt}\right)_\mu + \left(\frac{\partial c}{\partial t}\right)_{cum}$$

Rain water concentration, r

$$\frac{\partial r}{\partial t} = -h \frac{\partial r}{\partial h} + \left(\frac{dr}{dt}\right)_\mu + \frac{1}{\rho} \frac{\partial(\rho r V_t)}{\partial h}$$

Exner function (pressure) at the top, π_{top}

$$\frac{\partial \pi_{top}}{\partial t} = -u \frac{\partial \pi_{top}}{\partial x} + \frac{c_T g h}{\theta_v} + \left(\frac{\partial \pi_{top}}{\partial t} \right)_{cum}$$

Prognostic equations for the primitive equation model are summarized from Loveland.* The subscripts μ , and cum refer to the microphysical and cumulus parameterizations, respectively. In these equations, β is the "coordinate slope factor:" for heights $h < H$, $\beta(h) = 1 - \frac{h}{H}$; and for $h > H$, $\beta = 0$. E = terrain elevation above sea level (the height of level 1). h = vertical velocity where $h < H$. Note that for $h < H$, $h = \frac{z - E}{H - E} H$; and for $h > H$, $h = z$. See Loveland for more complete definitions.

*K. T. Loveland, 1980, Unpublished manuscripts on the two-dimensional, hydrostatic, primitive equation model, Department of Physics and Atmospheric Sciences, Drexel University, Philadelphia, PA

DIAGNOSTIC EQUATIONS

Hydrostatic (pressure)

$$\frac{\partial \pi}{\partial h} = \frac{\alpha g}{\theta_v} (1 + c + r); \quad p = p_0 \left(\frac{\pi}{C_p} \right)^{C_p/R}$$

Vertical velocity (continuity)

$$\frac{\partial(\dot{P}h)}{\partial h} = - \frac{\partial(Pu)}{\partial x} + p \left(\frac{1}{\theta_v} \frac{d\theta_v}{dt} + \frac{\dot{E}}{H - E} \right) \delta$$

$$\text{where } P = \frac{p}{\pi} \text{ and } \delta = \begin{cases} 1 & h < H \\ 0 & h \geq H \end{cases}$$

Temperature

$$T = \frac{\pi \theta_v}{C_p (1 + \epsilon^* q)} ;$$

$$\epsilon^* = \frac{R_v}{R_d} - 1 = 0.61$$

Equation of state (density)

$$\rho = \frac{C_p}{R} \frac{p}{\theta_v}$$

Diagnostic equations for the primitive equation model are summarized from Loveland.* In these equations α is the "coordinate compression factor": $\alpha(x)$ $= \frac{H - E}{H}$ for $h < H$ where E = terrain elevation above sea level, and $\alpha(x) = 1$ for $h > H$. $\dot{E} = \frac{dE}{dt}$. See Loveland for more complete definitions.

*K. T. Loveland, 1980, Unpublished manuscripts on the two-dimensional, hydrostatic, primitive equation model, Department of Physics and Atmospheric Sciences, Drexel University, Philadelphia, PA

DISTRIBUTION LIST

Commander
US Army Aviation Center
ATTN: ATZQ-D-MA
Fort Rucker, AL 36362

Chief, Atmospheric Sciences Div
Code ES-81
NASA
Marshall Space Flight Center, AL 35812

Commander
US Army Missile Command
ATTN: DRDMI-RRA/Dr. O. M. Essenwanger
Redstone Arsenal, AL 35809

Commander
US Army Missile Command
ATTN: DRSMI-OG (B. W. Fowler)
Redstone Arsenal, AL 35809

Commander
US Army Missile R&D Command
ATTN: DRDMI-TEM (R. Haraway)
Redstone Arsenal, AL 35809

Redstone Scientific Information Center
ATTN: DRSMI-RPRD (Documents)
US Army Missile Command
Redstone Arsenal, AL 35809

Commander
HQ, Fort Huachuca
ATTN: Tech Ref Div
Fort Huachuca, AZ 85613

Commander
US Army Intelligence
Center & School
ATTN: ATSI-CD-MD
Fort Huachuca, AZ 85613

Commander
US Army Yuma Proving Ground
ATTN: Technical Library
Bldg 2105
Yuma, AZ 85364

Dr. Frank D. Eaton
Geophysical Institute
University of Alaska
Fairbanks, AK 99701

Naval Weapons Center
Code 3918
ATTN: Dr. A. Shlanta
China Lake, CA 93555

Commanding Officer
Naval Envir Prediction Rsch Facility
ATTN: Library
Monterey, CA 93940

Sylvania Elec Sys Western Div
ATTN: Technical Reports Lib
PO Box 205
Mountain View, CA 94040

Geophysics Officer
PMTC Code 3250
Pacific Missile Test Center
Point Mugu, CA 93042

Commander
Naval Ocean Systems Center
(Code 4473)
ATTN: Technical Library
San Diego, CA 92152

Meteorologist in Charge
Kwajalein Missile Range
PO Box 67
APO San Francisco, CA 96555

Director
NOAA/ERL/APCL R31
RB3-Room 567
Boulder, CO 80302

Dr. B. A. Silverman D-1200
Office of Atmos Resources Management
Water and Power Resources Service
PO Box 25007 Denver Federal Center, Bldg. 67
Denver, CO 80225

Hugh W. Albers (Executive Secretary)
CAO Subcommittee on Atmos Rsch
National Science Foundation Room 510
Washington, DC 2055

Dr. Eugene W. Bierly
Director, Division of Atmos Sciences
National Science Foundation
1800 G Street, N.W.
Washington, DC 20550

Commanding Officer
Naval Research Laboratory
Code 2627
Washington, DC 20375

Defense Communications Agency
Technical Library Center
Code 222
Washington, DC 20305

Director
Naval Research Laboratory
Code 5530
Washington, DC 20375

Dr. J. M. MacCallum
Naval Research Laboratory
Code 1409
Washington, DC 20375

HQDA (DAEN-RDM/Dr. de Percin)
Washington, DC 20314

The Library of Congress
ATTN: Exchange & Gift Div
Washington, DC 20540
2

Mil Asst for Atmos Sci Ofc of
the Undersecretary of Defense
for Rsch & Engr/E&LS - RM 3D129
The Pentagon
Washington, DC 20301

AFATL/DLODL
Technical Library
Eglin AFB, FL 32542

Naval Training Equipment Center
ATTN: Technical Information Center
Orlando, FL 32813

Technical Library
Chemical Systems Laboratory
Aberdeen Proving Ground, MD 21010

US Army Materiel Systems
Analysis Activity
ATTN: DRXSY-MP
APG, MD 21005

Commander
ERADCOM
ATTN: DRDEL-PA/ILS/-ED
2800 Powder Mill Road
Adelphi, MD 20783

Commander
ERADCOM
ATTN: DRDEL-ST-T (Dr. B. Zarwyn)
2800 Powder Mill Road
Adelphi, MD 20783
02

Commander
Harry Diamond Laboratories
ATTN: DELHD-CO
2800 Powder Mill Road
Adelphi, MD 20783

Chief
Intel Mat Dev & Spt Ofc
ATTN: DELEW-WL-I
Bldg 4554
Fort George G. Mead, MD 20755

Acquisitions Section, IRDB-D823
Library & Info Svc Div, NOAA
6009 Executive Blvd.
Rockville, MD 20752

Naval Surface Weapons Center
White Oak Library
Silver Spring, MD 20910

Air Force Geophysics Laboratory
ATTN: LCC (A. S. Carten, Jr.)
Hanscom AFB, MA 01731

Air Force Geophysics Laboratory
ATTN: LYD
Hanscom AFB, MA 01731

Meteorology Division
AFGL/LY
Hanscom AFB, MA 01731

The Environmental Research
Institute of MI
ATTN: IRIA Library
PO Box 8618
Ann Arbor, MI 48107

Mr. William A. Main
USDA Forest Service
1407 S. Harrison Road
East Lansing, MI 48823

Dr. A. D. Belmont
Research Division
PO Box 1249
Control Data Corp
Minneapolis, MN 55440

Commander
Naval Oceanography Command
Bay St. Louis, MS 39529

Commanding Officer
US Army Armament R&D Command
ATTN: ORDAR-TSS Bldg 59
Dover, NJ 07801

Commander
ERADCOM Scientific Advisor
ATTN: DRDEL-SA
Fort Monmouth, NJ 07703

Commander
ERADCOM Tech Support Activity
ATTN: DELSD-L
Fort Monmouth, NJ 07703

Commander
HQ, US Army Avionics R&D Actv
ATTN: DAVAA-O
Fort Monmouth, NJ 07703

Commander
USA Elect Warfare Lab
ATTN: DELEW-DA (File Cy)
Fort Monmouth, NJ 07703

Commander
US Army Electronics R&D Command
ATTN: DELCS-S
Fort Monmouth, NJ 07703

Commander
US Army Satellite Comm Agency
ATTN: DRCPM-SC-3
Fort Monmouth, NJ 07703

Commander/Director
US Army Combat Survl & Target
Acquisition Laboratory
ATTN: DELCS-D
Fort Monmouth, NJ 07703

Director
Night Vision & Electro-Optics Laboratory
ATTN: DELNV-L (Dr. R. Buser)
Fort Belvoir, VA 22060

Project Manager, FIREFINDER
ATTN: DRCPM-FF
Fort Monmouth, NJ 07703

PM, Firefinder/REMBASS
ATTN: DRCPM-FFR-TM
Fort Monmouth, NJ 07703

6585 TG/WE
Holloman AFB, NM 88330

AFWL/Technical Library (SUL)
Kirtland AFB, NM 87117

AFWL/WE
Kirtland, AFB, NM 87117

TRASANA
ATTN: ATAA-SL (D. Anguiano)
WSMR, NM 88002

Commander
US Army White Sands Missile Range
ATTN: STEWS-PT-AL
White Sands Missile Range, NM 88002

Rome Air Development Center
ATTN: Documents Library
TSLD (Bette Smith)
Griffiss AFB, NY 13441

Environmental Protection Agency
Meteorology Laboratory, MD 80
Rsch Triangle Park, NC 27711

US Army Research Office
ATTN: DRXR0-PP
PO Box 12211
Rsch Triangle Park, NC 27709

Commandant
US Army Field Artillery School
ATTN: ATSF-CD-MS (Mr. Farmer)
Fort Sill, OK 73503

Commandant
US Army Field Artillery School
ATTN: ATSF-CF-R
Fort Sill, OK 73503

Commandant
US Army Field Artillery School
ATTN: Morris Swett Library
Fort Sill, OK 73503

Commander
US Army Dugway Proving Ground
ATTN: STEDP-MT-DA-M
(Mr. Paul Carlson)
Dugway, UT 84022

Commander
US Army Dugway Proving Ground
ATTN: MT-DA-L
Dugway, UT 84022

US Army Dugway Proving Ground
ATTN: STEDP-MT-DA-T
(Dr. W. A. Peterson)
Dugway, UT 84022

Inge Dirmhirn, Professor
Utah State University, UMC 48
Logan, UT 84322

Defense Technical Information Center
ATTN: DTIC-DDA-2
Cameron Station, Bldg. 5
Alexandria, VA 22314
12

Commanding Officer
US Army Foreign Sci & Tech Cen
ATTN: DRXST-IS1
220 7th Street, NE
Charlottesville, VA 22901

Naval Surface Weapons Center
Code G65
Dahlgren, VA 22448

Commander
US Army Night Vision
& Electro-Optics Lab
ATTN: DELNV-D
Fort Belvoir, VA 22060

Commander
USATRADO
ATTN: ATCD-FA
Fort Monroe, VA 23651

Commander
USATRADO
ATTN: ATCD-IR
Fort Monroe, VA 23651

Dept of the Air Force
5WW/DN
Langley AFB, VA 23665

US Army Nuclear & Cml Agency
ATTN: MONA-WE
Springfield, VA 22150

Director
US Army Signals Warfare Lab
ATTN: DELSW-OS (Dr. Burkhardt)
Vint Hill Farms Station
Warrenton, VA 22186

Commander
US Army Cold Regions Test Cen
ATTN: STECR-OP-PM
APO Seattle, WA 98733

ATMOSPHERIC SCIENCES RESEARCH PAPERS

1. Lindberg, J.D., "An Improvement to a Method for Measuring the Absorption Coefficient of Atmospheric Dust and other Strongly Absorbing Powders," ECOM-5565, July 1975.
2. Avara, Elton P., "Mesoscale Wind Shears Derived from Thermal Winds," ECOM-5566, July 1975.
3. Gomez, Richard B., and Joseph H. Pierluissi, "Incomplete Gamma Function Approximation for King's Strong-Line Transmittance Model," ECOM-5567, July 1975.
4. Blanco, A.J., and B.F. Engelos, "Ballistic Wind Weighting Functions for Tank Projectiles," ECOM-5568, August 1975.
5. Taylor, Fredrick J., Jack Smith, and Thomas H. Pries, "Crosswind Measurements through Pattern Recognition Techniques," ECOM-5569, July 1975.
6. Walters, D.L., "Crosswind Weighting Functions for Direct-Fire Projectiles," ECOM-5570, August 1975.
7. Duncan, Louis D., "An Improved Algorithm for the Iterated Minimal Information Solution for Remote Sounding of Temperature," ECOM-5571, August 1975.
8. Robbiani, Raymond L., "Tactical Field Demonstration of Mobile Weather Radar Set AN TPS-11 at Fort Rucker, Alabama," ECOM-5572, August 1975.
9. Miers, B., G. Blackman, D. Langer, and N. Lorimier, "Analysis of SMS/GOES Film Data," ECOM-5573, September 1975.
10. Manquero, Carlos, Louis Duncan, and Rufus Bruce, "An Indication from Satellite Measurements of Atmospheric CO₂ Variability," ECOM-5574, September 1975.
11. Petraceca, Carmine, and James D. Lindberg, "Installation and Operation of an Atmospheric Particulate Collector," ECOM-5575, September 1975.
12. Avara, Elton P., and George Alexander, "Empirical Investigation of Three Iterative Methods for Inverting the Radiative Transfer Equation," ECOM-5576, October 1975.
13. Alexander, George D., "A Digital Data Acquisition Interface for the SMS Direct Readout Ground Station - Concept and Preliminary Design," ECOM-5577, October 1975.
14. Cantor, Israel, "Enhancement of Point Source Thermal Radiation Under Clouds in a Nonattenuating Medium," ECOM 5578, October 1975.
15. Norton, Colburn, and Glenn Hoidale, "The Diurnal Variation of Mixing Height by Month over White Sands Missile Range, N.M.," ECOM-5579, November 1975.
16. Avara, Elton P., "On the Spectrum Analysis of Binary Data," ECOM-5580, November 1975.
17. Taylor, Fredrick J., Thomas H. Pries, and Chao-Huan Huang, "Optimal Wind Velocity Estimation," ECOM-5581, December 1975.
18. Avara, Elton P., "Some Effects of Autocorrelated and Cross-Correlated Noise on the Analysis of Variance," ECOM-5582, December 1975.
19. Gillespie, Patti S., R.L. Armstrong, and Kenneth O. White, "The Spectral Characteristics and Atmospheric CO₂ Absorption of the Ho⁺ YLF Laser at 2.05 μ m," ECOM-5583, December 1975.
20. Novlan, David J., "An Empirical Method of Forecasting Thunderstorms for the White Sands Missile Range," ECOM-5584, February 1976.
21. Avara, Elton P., "Randomization Effects in Hypothesis Testing with Autocorrelated Noise," ECOM-5585, February 1976.
22. Watkins, Wendell R., "Improvements in Long Path Absorption Cell Measurement," ECOM-5586, March 1976.
23. Thomas, Joe, George D. Alexander, and Marvin Dubbin, "SATTEL - An Army Dedicated Meteorological Telemetry System," ECOM-5587, March 1976.
24. Kennedy, Bruce W., and Delbert Bynum, "Army User Test Program for the RDT&E-XM-75 Meteorological Rocket," ECOM-5588, April 1976.

25. Barnett, Kenneth M., "A Description of the Artillery Meteorological Comparisons at White Sands Missile Range, October 1974 - December 1974 ('PASS' - Prototype Artillery [Meteorological] Subsystem)," ECOM-5589, April 1976.
26. Miller, Walter B., "Preliminary Analysis of Fall-of-Shot From Project 'PASS'," ECOM-5590, April 1976.
27. Avara, Elton P., "Error Analysis of Minimum Information and Smith's Direct Methods for Inverting the Radiative Transfer Equation," ECOM-5591, April 1976.
28. Yee, Young P., James D. Horn, and George Alexander, "Synoptic Thermal Wind Calculations from Radiosonde Observations Over the Southwestern United States," ECOM-5592, May 1976.
29. Duncan, Louis D., and Mary Ann Seagraves, "Applications of Empirical Corrections to NOAA-4 VTPR Observations," ECOM-5593, May 1976.
30. Miers, Bruce T., and Steve Weaver, "Applications of Meteorological Satellite Data to Weather Sensitive Army Operations," ECOM-5594, May 1976.
31. Sharenow, Moses, "Redesign and Improvement of Balloon ML-566," ECOM-5595, June, 1976.
32. Hansen, Frank V., "The Depth of the Surface Boundary Layer," ECOM-5596, June 1976.
33. Pinnick, R.G., and E.B. Stenmark, "Response Calculations for a Commercial Light-Scattering Aerosol Counter," ECOM-5597, July 1976.
34. Mason, J., and G.B. Hoidale, "Visibility as an Estimator of Infrared Transmittance," ECOM-5598, July 1976.
35. Bruce, Rufus E., Louis D. Duncan, and Joseph H. Pierluissi, "Experimental Study of the Relationship Between Radiosonde Temperatures and Radiometric-Area Temperatures," ECOM-5599, August 1976.
36. Duncan, Louis D., "Stratospheric Wind Shear Computed from Satellite Thermal Sounder Measurements," ECOM-5800, September 1976.
37. Taylor, F., P. Mohan, P. Joseph and T. Pries, "An All Digital Automated Wind Measurement System," ECOM-5801, September 1976.
38. Bruce, Charles, "Development of Spectrophones for CW and Pulsed Radiation Sources," ECOM-5802, September 1976.
39. Duncan, Louis D., and Mary Ann Seagraves, "Another Method for Estimating Clear Column Radiances," ECOM-5803, October 1976.
40. Blanco, Abel J., and Larry E. Taylor, "Artillery Meteorological Analysis of Project Pass," ECOM-5804, October 1976.
41. Miller, Walter, and Bernard Engebos, "A Mathematical Structure for Refinement of Sound Ranging Estimates," ECOM-5805, November, 1976.
42. Gillespie, James B., and James D. Lindberg, "A Method to Obtain Diffuse Reflectance Measurements from 1.0 to 3.0 μ m Using a Cary 171 Spectrophotometer," ECOM-5806, November 1976.
43. Rubio, Roberto, and Robert O. Olsen, "A Study of the Effects of Temperature Variations on Radio Wave Absorption," ECOM-5807, November 1976.
44. Ballard, Harold N., "Temperature Measurements in the Stratosphere from Balloon-Borne Instrument Platforms, 1968-1975," ECOM-5808, December 1976.
45. Monahan, H.H., "An Approach to the Short-Range Prediction of Early Morning Radiation Fog," ECOM-5809, January 1977.
46. Engebos, Bernard Francis, "Introduction to Multiple State Multiple Action Decision Theory and Its Relation to Mixing Structures," ECOM-5810, January 1977.
47. Low, Richard D.H., "Effects of Cloud Particles on Remote Sensing from Space in the 10-Micrometer Infrared Region," ECOM-5811, January 1977.
48. Bonner, Robert S., and R. Newton, "Application of the AN/GVS-5 Laser Rangefinder to Cloud Base Height Measurements," ECOM-5812, February 1977.
49. Rubio, Roberto, "Lidar Detection of Subvisible Reentry Vehicle Erosive Atmospheric Material," ECOM-5813, March 1977.
50. Low, Richard D.H., and J.D. Horn, "Mesoscale Determination of Cloud-Top Height: Problems and Solutions," ECOM-5814, March 1977.

51. Duncan, Louis D., and Mary Ann Seagraves, "Evaluation of the NOAA-4 VTPR Thermal Winds for Nuclear Fallout Predictions," ECOM-5815, March 1977.
52. Randhawa, Jagr S., M. Izquierdo, Carlos McDonald and Zvi Salpeter, "Stratospheric Ozone Density as Measured by a Chemiluminescent Sensor During the Stratcom VI-A Flight," ECOM-5816, April 1977.
53. Rubio, Roberto, and Mike Izquierdo, "Measurements of Net Atmospheric Irradiance in the 0.7- to 2.8-Micrometer Infrared Region," ECOM-5817, May 1977.
54. Ballard, Harold N., Jose M. Serna, and Frank P. Hudson Consultant for Chemical Kinetics, "Calculation of Selected Atmospheric Composition Parameters for the Mid-Latitude, September Stratosphere," ECOM-5818, May 1977.
55. Mitchell, J.D., R.S. Sagar, and R.O. Olsen, "Positive Ions in the Middle Atmosphere During Sunrise Conditions," ECOM-5819, May 1977.
56. White, Kenneth O., Wendell R. Watkins, Stuart A. Schleusener, and Ronald L. Johnson, "Solid-State Laser Wavelength Identification Using a Reference Absorber," ECOM-5820, June 1977.
57. Watkins, Wendell R., and Richard G. Dixon, "Automation of Long-Path Absorption Cell Measurements," ECOM-5821, June 1977.
58. Taylor, S.E., J.M. Davis, and J.B. Mason, "Analysis of Observed Soil Skin Moisture Effects on Reflectance," ECOM-5822, June 1977.
59. Duncan, Louis D. and Mary Ann Seagraves, "Fallout Predictions Computed from Satellite Derived Winds," ECOM-5823, June 1977.
60. Snider, D.E., D.G. Murcray, F.H. Murcray, and W.J. Williams, "Investigation of High-Altitude Enhanced Infrared Background Emissions" (U), SECRET, ECOM-5824, June 1977.
61. Dubbin, Marvin H. and Dennis Hall, "Synchronous Meteorological Satellite Direct Readout Ground System Digital Video Electronics," ECOM-5825, June 1977.
62. Miller, W., and B. Engebos, "A Preliminary Analysis of Two Sound Ranging Algorithms," ECOM-5826, July 1977.
63. Kennedy, Bruce W., and James K. Luers, "Ballistic Sphere Techniques for Measuring Atmospheric Parameters," ECOM-5827, July 1977.
64. Duncan, Louis D., "Zenith Angle Variation of Satellite Thermal Sounder Measurements," ECOM-5828, August 1977.
65. Hansen, Frank V., "The Critical Richardson Number," ECOM-5829, September 1977.
66. Ballard, Harold N., and Frank P. Hudson (Compilers), "Stratospheric Composition Balloon-Borne Experiment," ECOM-5830, October 1977.
67. Barr, William C., and Arnold C. Peterson, "Wind Measuring Accuracy Test of Meteorological Systems," ECOM-5831, November 1977.
68. Ethridge, G.A. and F.V. Hansen, "Atmospheric Diffusion: Similarity Theory and Empirical Derivations for Use in Boundary Layer Diffusion Problems," ECOM-5832, November 1977.
69. Low, Richard D.H., "The Internal Cloud Radiation Field and a Technique for Determining Cloud Blackness," ECOM-5833, December 1977.
70. Watkins, Wendell R., Kenneth O. White, Charles W. Bruce, Donald L. Walters, and James D. Lindberg, "Measurements Required for Prediction of High Energy Laser Transmission," ECOM-5834, December 1977.
71. Rubio, Robert, "Investigation of Abrupt Decreases in Atmospherically Backscattered Laser Energy," ECOM-5835, December 1977.
72. Monahan, H.H. and R.M. Cionco, "An Interpretative Review of Existing Capabilities for Measuring and Forecasting Selected Weather Variables (Emphasizing Remote Means)," ASL-TR-0001, January 1978.
73. Heaps, Melvin G., "The 1979 Solar Eclipse and Validation of D-Region Models," ASL-TR-0002, March 1978.

74. Jennings, S.G., and J.B. Gillespie, "M.I.E. Theory Sensitivity Studies - The Effects of Aerosol Complex Refractive Index and Size Distribution Variations on Extinction and Absorption Coefficients Part II: Analysis of the Computational Results," ASL-TR-0003, March 1978.
75. White, Kenneth O. et al, "Water Vapor Continuum Absorption in the 3.5 μ m to 4.0 μ m Region," ASL-TR-0004, March 1978.
76. Olsen, Robert O., and Bruce W. Kennedy, "ABRES Pretest Atmospheric Measurements," ASL-TR-0005, April 1978.
77. Ballard, Harold N., Jose M. Serna, and Frank P. Hudson, "Calculation of Atmospheric Composition in the High Latitude September Stratosphere," ASL-TR-0006, May 1978.
78. Watkins, Wendell R. et al, "Water Vapor Absorption Coefficients at HF Laser Wavelengths," ASL-TR-0007, May 1978.
79. Hansen, Frank V., "The Growth and Prediction of Nocturnal Inversions," ASL-TR-0008, May 1978.
80. Samuel, Christine, Charles Bruce, and Ralph Brewer, "Spectrophone Analysis of Gas Samples Obtained at Field Site," ASL-TR-0009, June 1978.
81. Pinnick, R.G. et al., "Vertical Structure in Atmospheric Fog and Haze and its Effects on IR Extinction," ASL-TR-0010, July 1978.
82. Low, Richard D.H., Louis D. Duncan, and Richard B. Gomez, "The Microphysical Basis of Fog Optical Characterization," ASL-TR-0011, August 1978.
83. Heaps, Melvin G., "The Effect of a Solar Proton Event on the Minor Neutral Constituents of the Summer Polar Mesosphere," ASL-TR-0012, August 1978.
84. Mason, James B., "Light Attenuation in Falling Snow," ASL-TR-0013, August 1978.
85. Blanco, Abel J., "Long-Range Artillery Sound Ranging: "PASS" Meteorological Application," ASL-TR-0014, September 1978.
86. Heaps, M.G., and F.E. Niles, "Modeling the Ion Chemistry of the D-Region: A case Study Based Upon the 1966 Total Solar Eclipse," ASL-TR-0015, September 1978.
87. Jennings, S.G., and R.G. Pinnick, "Effects of Particulate Complex Refractive Index and Particle Size Distribution Variations on Atmospheric Extinction and Absorption for Visible Through Middle-Infrared Wavelengths," ASL-TR-0016, September 1978.
88. Watkins, Wendell R., Kenneth O. White, Lanny R. Bower, and Brian Z. Sojka, "Pressure Dependence of the Water Vapor Continuum Absorption in the 3.5- to 4.0-Micrometer Region," ASL-TR-0017, September 1978.
89. Miller, W.B., and B.F. Engebos, "Behavior of Four Sound Ranging Techniques in an Idealized Physical Environment," ASL-TR-0018, September 1978.
90. Gomez, Richard G., "Effectiveness Studies of the CBU-88/B Bomb, Cluster, Smoke Weapon" (U), CONFIDENTIAL ASL-TR-0019, September 1978.
91. Miller, August, Richard C. Shirkey, and Mary Ann Seagraves, "Calculation of Thermal Emission from Aerosols Using the Doubling Technique," ASL-TR-0020, November, 1978.
92. Lindberg, James D. et al., "Measured Effects of Battlefield Dust and Smoke on Visible, Infrared, and Millimeter Wavelengths Propagation: A Preliminary Report on Dusty Infrared Test-I (DIRT-I)," ASL-TR-0021, January 1979.
93. Kennedy, Bruce W., Arthur Kinghorn, and B.R. Hixon, "Engineering Flight Tests of Range Meteorological Sounding System Radiosonde," ASL-TR-0022, February 1979.
94. Rubio, Roberto, and Don Hooek, "Microwave Effective Earth Radius Factor Variability at Wiesbaden and Balboa," ASL-TR-0023, February 1979.
95. Low, Richard D.H., "A Theoretical Investigation of Cloud/Fog Optical Properties and Their Spectral Correlations," ASL-TR-0024, February 1979.

96. Pinnick, R.G., and H.J. Auvermann, "Response Characteristics of Knollenberg Light-Scattering Aerosol Counters," ASL-TR-0025, February 1979.
97. Heaps, Melvin G., Robert O. Olsen, and Warren W. Berning, "Solar Eclipse 1979, Atmospheric Sciences Laboratory Program Overview," ASL-TR-0026 February 1979.
98. Blanco, Abel J., "Long-Range Artillery Sound Ranging: 'PASS' GR-8 Sound Ranging Data," ASL-TR-0027, March 1979.
99. Kennedy, Bruce W., and Jose M. Serna, "Meteorological Rocket Network System Reliability," ASL-TR-0028, March 1979.
100. Swingle, Donald M., "Effects of Arrival Time Errors in Weighted Range Equation Solutions for Linear Base Sound Ranging," ASL-TR-0029, April 1979.
101. Umstead, Robert K., Ricardo Pena, and Frank V. Hansen, "KWIK: An Algorithm for Calculating Munition Expenditures for Smoke Screening/Obscuration in Tactical Situations," ASL-TR-0030, April 1979.
102. D'Arcy, Edward M., "Accuracy Validation of the Modified Nike Hercules Radar," ASL-TR-0031, May 1979.
103. Rodriguez, Ruben, "Evaluation of the Passive Remote Crosswind Sensor," ASL-TR-0032, May 1979.
104. Barber, T.L., and R. Rodriguez, "Transit Time Lidar Measurement of Near-Surface Winds in the Atmosphere," ASL-TR-0033, May 1979.
105. Low, Richard D.H., Louis D. Duncan, and Y.Y. Roger R. Hsiao, "Microphysical and Optical Properties of California Coastal Fogs at Fort Ord," ASL-TR-0034, June 1979.
106. Rodriguez, Ruben, and William J. Vechione, "Evaluation of the Saturation Resistant Crosswind Sensor," ASL-TR-0035, July 1979.
107. Ohmstede, William D., "The Dynamics of Material Layers," ASL-TR-0036, July 1979.
108. Pinnick, R.G., S.G. Jennings, Petr Chylek, and H.J. Auvermann "Relationships between IR Extinction, Absorption, and Liquid Water Content of Fogs," ASL-TR-0037, August 1979.
109. Rodriguez, Ruben, and William J. Vechione, "Performance Evaluation of the Optical Crosswind Profiler," ASL-TR-0038, August 1979.
110. Miers, Bruce T., "Precipitation Estimation Using Satellite Data" ASL-TR-0039, September 1979.
111. Dickson, David H., and Charles M. Sonnenschein, "Helicopter Remote Wind Sensor System Description," ASL-TR-0040, September 1979.
112. Heaps, Melvin, G., and Joseph M. Heimerl, "Validation of the Dairchem Code, I: Quiet Midlatitude Conditions," ASL-TR-0041, September 1979.
113. Bonner, Robert S., and William J. Lentz, "The Visioceilometer: A Portable Cloud Height and Visibility Indicator," ASL-TR-0042, October 1979.
114. Cohn, Stephen L., "The Role of Atmospheric Sulfates in Battlefield Obscurations," ASL-TR-0043, October 1979.
115. Fawbush, E.J. et al, "Characterization of Atmospheric Conditions at the High Energy Laser System Test Facility (HELSTF), White Sands Missile Range, New Mexico, Part I, 24 March to 8 April 1977," ASL-TR-0044, November 1979.
116. Barber, Ted L., "Short-Time Mass Variation in Natural Atmospheric Dust," ASL-TR-0045, November 1979.
117. Low, Richard D.H., "Fog Evolution in the Visible and Infrared Spectral Regions and its Meaning in Optical Modeling," ASL-TR-0046, December 1979.
118. Duncan, Louis D. et al, "The Electro-Optical Systems Atmospheric Effects Library, Volume I: Technical Documentation, ASL-TR-0047, December 1979.
119. Shirkey, R. C. et al, "Interim E-O SAEL, Volume II, Users Manual," ASL-TR-0048, December 1979.
120. Kobayashi, H.K., "Atmospheric Effects on Millimeter Radio Waves," ASL-TR-0049, January 1980.
121. Seagraves, Mary Ann and Duncan, Louis D., "An Analysis of Transmittances Measured Through Battlefield Dust Clouds," ASL-TR-0050, February 1980.

122. Dickson, David H., and Jon E. Ottesen, "Helicopter Remote Wind Sensor Flight Test," ASL-TR-0051, February 1980.
123. Pinnick, R. G., and S. G. Jennings, "Relationships Between Radiative Properties and Mass Content of Phosphoric Acid, HC, Petroleum Oil, and Sulfuric Acid Military Smokes," ASL-TR-0052, April 1980.
124. Hinds, B. D., and J. B. Gillespie, "Optical Characterization of Atmospheric Particulates on San Nicolas Island, California," ASL-TR-0053, April 1980.
125. Miers, Bruce T., "Precipitation Estimation for Military Hydrology," ASL-TR-0054, April 1980.
126. Stenmark, Ernest B., "Objective Quality Control of Artillery Computer Meteorological Messages," ASL-TR-0055, April 1980.
127. Duncan, Louis D., and Richard D. H. Low, "Bimodal Size Distribution Models for Fogs at Meppen, Germany," ASL-TR-0056, April 1980.
128. Olsen, Robert O., and Jagir S. Randhawa, "The Influence of Atmospheric Dynamics on Ozone and Temperature Structure," ASL-TR-0057, May 1980.
129. Kennedy, Bruce W., et al, "Dusty Infrared Test-II (DIRT-II) Program," ASL-TR-0058, May 1980.
130. Heaps, Melvin G., Roberts O. Olsen, Warren Berning, John Cross, and Arthur Gilcrease, "1979 Solar Eclipse, Part I - Atmospheric Sciences Laboratory Field Program Summary," ASL-TR-0059, May 1980.
131. Miller, Walter B., "User's Guide for Passive Target Acquisition Program Two (PTAP-2)," ASL-TR-0060, June 1980.
132. Holt, E. H., H. H. Monahan, and E. J. Fawbush, "Atmospheric Data Requirements for Battlefield Obscuration Applications," ASL-TR-0061, June 1980.
133. Shirkey, Richard C., August Miller, George H. Goedecke, and Yugal Behl, "Single Scattering Code AGAUSX: Theory, Applications, Comparisons, and Listing," ASL-TR-0062, July 1980.
134. Sojka, Brain Z., and Kenneth O. White, "Evaluation of Specialized Photoacoustic Absorption Chambers for Near-millimeter Wave (NMMW) Propagation Measurements," ASL-TR-0063, August 1980.
135. Bruce, Charles W., Young Paul Yee, and S. G. Jennings, "In Situ Measurement of the Ratio of Aerosol Absorption to Extinction Coefficient," ASL-TR-0064, August 1980.
136. Yee, Young Paul, Charles W. Bruce, and Ralph J. Brewer, "Gaseous/Particulate Absorption Studies at WSMR using Laser Sourced Spectrophones," ASL-TR-0065, June 1980.
137. Lindberg, James D., Radon B. Loveland, Melvin Heaps, James B. Gillespie, and Andrew F. Lewis, "Battlefield Dust and Atmospheric Characterization Measurements During West German Summertime Conditions in Support of Grafenwohr Tests," ASL-TR-0066, September 1980.
138. Vechione, W. J., "Evaluation of the Environmental Instruments, Incorporated Series 200 Dual Component Wind Set," ASL-TR-0067, September 1980.
139. Bruce, C. W., Y. P. Yee, B. D. Hinds, R. G. Pinnick, R. J. Brewer, and J. Minjares, "Initial Field Measurements of Atmospheric Absorption at 9 μ m to 11 μ m Wavelengths," ASL-TR-0068, October 1980.
140. Heaps, M. G., R. O. Olsen, K. D. Baker, D. A. Burt, L. C. Howlett, L. L. Jensen, E. F. Pound, and G. D. Allred, "1979 Solar Eclipse: Part II Initial Results for Ionization Sources, Electron Density, and Minor Neutral Constituents," ASL-TR-0069, October 1980.
141. Low, Richard D. H., "One-Dimensional Cloud Microphysical Models for Central Europe and their Optical Properties," ASL-TR-0070, October 1980.
142. Duncan, Louis D., James D. Lindberg, and Radon B. Loveland, "An Empirical Model of the Vertical Structure of German Fogs," ASL-TR-0071, November 1980.

143. Duncan, Louis D., 1981, "EOSAFL 80, Volume I, Technical Documentation," ASL-TR-0072, January 1981.
144. Shirkey, R. C., and S. G. O'Brien, "EOSAEL 80, Volume II, Users Manual," ASL-TR-0073, January 1981.
145. Bruce, C. W., "Characterization of Aerosol Nonlinear Effects on a High-Power CO₂ Laser Beam," ASL-TR-0074 (Draft), February 1981.
146. Duncan, Louis D., and James D. Lindberg, "Air Mass Considerations in Fog Optical Modeling," ASL-TR-0075, February 1981.
147. Kunkel, Kenneth E., "Evaluation of a Tethered Kite Anemometer," ASL-TR-0076, February 1981.
148. Kunkel, K. E., et al, "Characterization of Atmospheric Conditions at the High Energy Laser System Test Facility (HELSTF) White Sands Missile Range, New Mexico, August 1977 to October 1978, Part II, Optical Turbulence, Wind, Water Vapor Pressure, Temperature," ASL-TR-0077, February 1981.
149. Miers, Bruce T., "Weather Scenarios for Central Germany," ASL-TR-0078, February 1981.
150. Cogan, James L., "Sensitivity Analysis of a Mesoscale Moisture Model," ASL-TR-0079, March 1981.

